RSC Advances

PAPER

View Article Online
View Journal | View Issue

Cite this: *RSC Adv.*, 2026, **16**, 14638

A structural blueprint for antibacterial discovery: microwave- and ultrasound-assisted synthesis of pyrrolidine-fused quinoxalines as novel inhibitors of DNA gyrase and biofilm

Eman A. Fayed, *[a] Mazin A. A. Najm,[b] Mostafa I. Abdelglil,[c] Triveena M. Ramsis,*[d] Nirvana A. Gohar,[e] Shimaa A. Metwally[f] and Maha A. Ebrahim[a]

In order to lessen the severity of infectious diseases, anti-infective agents—drugs that prevent, combat, or control infections brought on by microorganisms—are essential in contemporary medicine. To tackle antimicrobial resistance, this project intends to design and synthesize hybrid compounds that contain pyrrolidine, quinoxaline and a hydrazinyl bridge, and assess the antimicrobial and antifungal properties of these compounds against a variety of pathogenic strains. The bactericidal properties of hybrids **24**, **27**, and **29** against *E. coli* were verified. The MIC of 12.5 μM was shown by hybrids **24**, **25**, and **31**, which suggests bactericidal hybrids are effective against *P. aeruginosa* at greater concentrations. In comparison to Levofloxacin, treatment with all hybrids produced an 89–92% reduction in biofilm formation at 90% MIC. Eight hybrids' killing kinetics against *P. aeruginosa* were time-dependent, with an abrupt decrease in CFU number observed at higher concentrations. While 4-fold and 8-fold MICs resulted in nearly total bacterial eradication, primary bacterial elimination happened after three hours. The most effective DNA gyrase inhibitors were hybrids **25**, **28**, and **31**; their IC_{50} values were significantly less than that of ciprofloxacin (77.3, 87.6, and 65.5 μM, respectively). To determine the best drug-like qualities, the study examined the physicochemical and pharmacokinetic features of active compounds. Molecular docking simulation experiments were also conducted to comprehend the binding interactions and mechanisms of action of these hits.

Received 25th January 2026
Accepted 11th March 2026

DOI: 10.1039/d6ra00675b

rsc.li/rsc-advances

1. Introduction

Diseases caused by infectious bacteria, viruses, and fungi have appeared and are continuing to grow in tandem with daily life.[1–4] The need for novel antimicrobial drugs with lower toxicity and resistance strain activity appears unresolved.[5–8]

Although many antibacterial medications are already accessible, microorganism resistance to antibiotics remains an immense issue.[9–12] Compounds that are heterocyclic are frequently included in numerous synthetic and biological fields because of their ubiquitous occurrence in nature.[13–16] Amongst the several scaffolds considered for the prospective pharmacological applications of them, nitrogen-containing heterocyclic frameworks have acquired a lot of focus owing to the diverse spectrum of biological processes,[17–19] comprising antifungal,[20,21] antimicrobial,[22,23] anticancer,[24,25] antiviral,[26,27] and antidiabetic properties.[28,29]

A useful pharmacophore in medicinal science, quinoxaline, is a bicyclic molecule constructed when a pyrazine ring and a benzene ring combine.[30–33] Its distinct structure permits a variety of alterations, producing molecules with ameliorated biological activity.[34–37] Due to its capacity to communicate with the essential cellular structures and microbial enzymes, quinoxaline derivatives have recently been shown to potentially be potent antimicrobial drugs.[38] The naturally occurring antibiotic phenazinomycin, which has anticancer properties, is another antibacterial medication containing a quinoxaline scaffold.[39–43]

Additionally, pyrrolidine ring piqued the curiosity of scientists because of its strong antibacterial qualities.[44–47] Numerous quinolone antibiotics, including Gemifloxcin and Moxifloxacin, include pyrrolidine.[48–50] In addition, the newly approved drug vonoprazan, which destroys *Helicobacter-pylori*, has a scaffold

[a]*Department of Pharmaceutical Organic Chemistry, Faculty of Pharmacy (Girls), Al-Azhar University, Cairo 11754, Egypt. E-mail: alfayed_e@azhar.edu.eg; alfayed_e@yahoo.com; Tel: +202 01221330523*

[b]*Department of Pharmacy, Mazaya University College, Nasiriyah 64001, Iraq*

[c]*Department of Medical Laboratory Techniques, Al-Farahidi University, Baghdad, 10021, Iraq*

[d]*Department of Pharmaceutical Chemistry, Faculty of Pharmacy, Sinai University, Kantara Branch, Ismailia 41636, Egypt. E-mail: triveena.farid@su.edu.eg; triveenaramsis@gmail.com*

[e]*Department of Pharmaceutical Organic Chemistry, Faculty of Pharmacy, Modern University for Technology and Information (MTI), Cairo 11571, Egypt*

[f]*Microbiology and Immunology Department Faculty of Pharmacy (Girls), Al-Azhar University, Cairo 11754, Egypt*

with a pyrrole ring.[51–53] Including an azo part to the compounds which are heterocyclic enhances the drug's biological impact.[27,54–57]

DNA gyrase is a potential target for antibacterial therapy, a crucial bacterial enzyme associated with transcription, recombination, and DNA replication.[58] The effective prevention of bacterial growth is achieved by DNA gyrase inhibitors, which disrupt DNA supercoiling and replication.[59] Since DNA gyrase is essential for bacterial life yet is absent from human cells, it is a desirable target for targeted antimicrobial therapy.[60]

The notion that bacteria must attain a particular cell density in infectious illnesses before they may establish virulence factors and interfere with the host defences is widely recognized.[61,62] Pathogenic bacteria have evolved a special mechanism known as "biofilm formation" to withstand the lethal assaults of oxidative stress, nutritional deprivation, and the host immune system or antibiotics. Microorganisms form a biofilm while they latch on to an abiotic or biotic surface in a matrix of extracellular polymeric substance (EPS). The ability of *Candida* species forge biofilms, in addition to bacteria, increases the possibility of resistance to existing antifungal medications.[63,64] The need for novel molecules or hybrids of already-existing chemicals that can suppress or destroy the biofilm matrix is critical because there is currently no treatment option for biofilms in clinical settings.

The purpose of this work is to use pyrrolidine-fused quinoxaline employing azo bridge to produce a variety of novel hybrid compounds, as seen in Fig. 1. The evaluation of the novel hybrids involved examining their DNA gyrase inhibitory, antibacterial, and antifungal properties. The antibiofilm activity of each bactericidal derivative was examined. Each compound was examined for pharmacokinetic and physicochemical characteristics. Lastly, an evaluation of binding mode simulations through docking for the most successful samples were carried out.

2. Findings and analysis

2.1. Chemical synthesis

The methods indicated in Schemes 1–3 were used to synthesis the target compounds.

Benzene-1,2-diamine **1** was relfuxed with oxalic acid **2** using water as a solvent in presence of conc. HCl affording 1,4-dihydroquinoxaline-2,3-dione **3**. Further reaction of **3** with thionyl chloride resulted in 2,3-dichloroquinoxaline **5**. Hydrazinylquinoxaline **4** or **6** were obtained by refluxing **3** or **5** with hydrated-hydrazine, respectively, in ethyl alcohol for 24 h, accordingly as represented in Scheme 1.[65]

Furthermore, the reaction of itaconic acid **7** with various aniline derivatives **8–15**, afforded the 5-oxo-pyrrolidine derivatives **16–23** (Scheme 2). The reaction was conducted using three methods implementing the principles of green chemistry (discussed in the experimental section). Using ultrasound-assisted reaction afforded the highest yield and consumed the least time. The reaction time and yield are given in Table 1. Structure elucidation using ^{1}H NMR confirmed the structures of oxo-pyrrolidine derivatives **16–23**. The COOH proton appeared as a singlet-signal at approximately δ 12 part per million (ppm). The hydrogens for the two methylene carbons appeared as four doublet of doublet signals each integrating one proton at approximately δ 2 and 4 ppm. The methine hydrogens from pyrrolidine showed up as a multiplet at approximately delta-(δ) 3 ppm.

The targeted quinoxalne-pyrrolidine hybrids **24–31** were afforded by refluxing the respective pyrrolidine fragment with hydrazinyl quinoxaline **4** or **6** (Scheme 3). A characteristic singlet appeared in the ^{1}H NMR spectra of hybrids **24–27** at approximately δ 11–12 ppm representing the 2-OH proton on the quinoxaline ring. In all synthesized hybrids, –NH–**NH**–CO showed as doublet at δ 11 ppm, while –**NH**–NH–CO showed as a doublet roughly between δ 5 and 8 ppm. The protons of the pyrrolidine ring exhibited the identical signal pattern in all

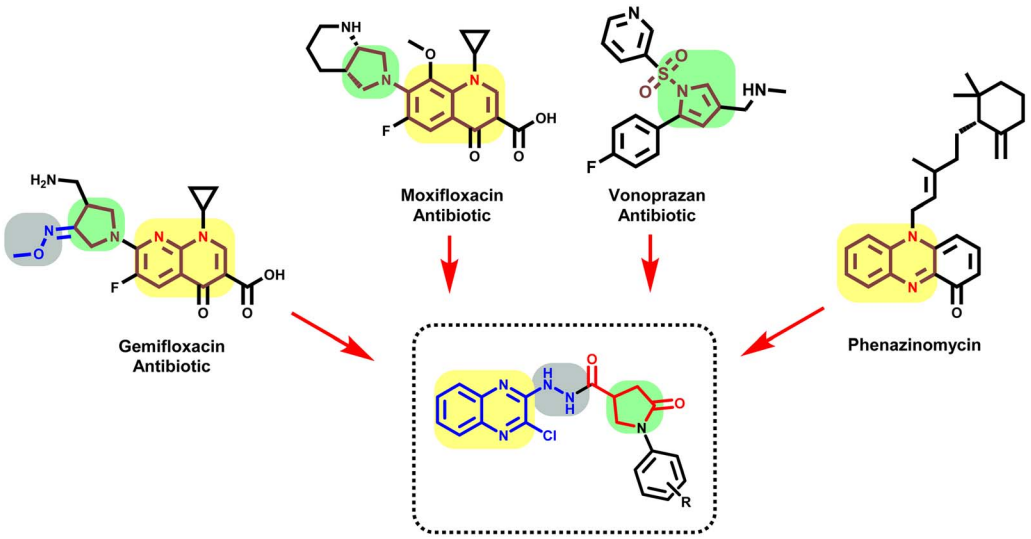

Fig. 1 Schematic representation of hybridized substances featuring quinoxaline, pyrrole/pyrrolidine, azo-bridge, and various substitutes.

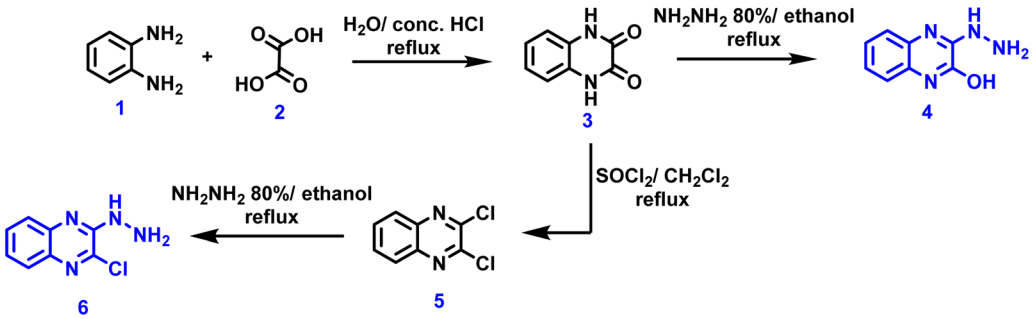

Scheme 1 Creation of hydrazinylquinoxaline (**4**) and (**6**).

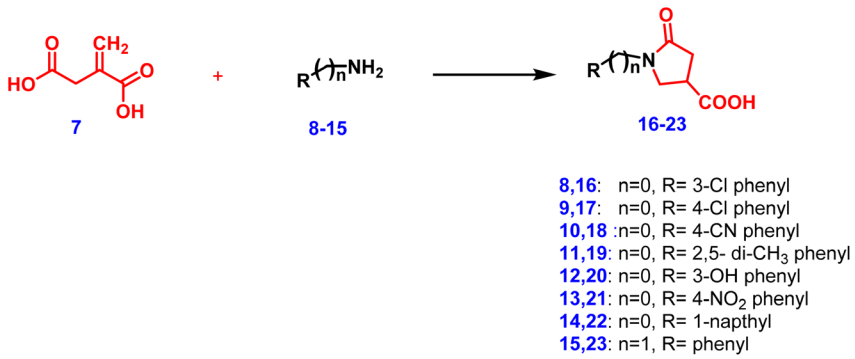

Scheme 2 Manufacturing of oxo-pyrrolidine fragments **16–23**.

synthesized hybrids. The ^{13}C NMR of all synthesized hybrids revealed two characteristic signals representing the two C=O groups at δ between 170 and 175 ppm.

The ^{1}H NMR of hybrids **25** and **29** demonstrated two characteristic signals between δ 2 and 2.3 ppm, each integrating for 3 protons representing the two methyl groups. Additionally, the two methyl groups were shown as two signals in ^{13}C NMR at approximately δ 16 and 19 ppm. The ^{1}H NMR of hybrids **26** and **30** a signal representing the phenolic-OH between delta (δ) 7 and delta (δ) 8 part per million. The ^{13}C NMR of hybrids **24** and **28** confirmed the presence of the cyano groups at approximately δ 118 ppm.

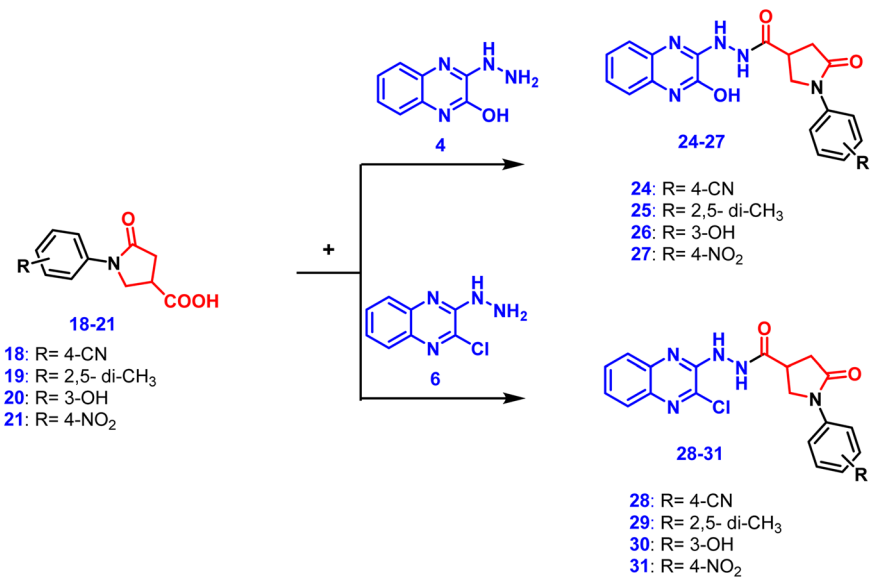

Scheme 3 Preparation of quinoxaline–pyrrolidine conjugates **24–31**.

Table 1 Effect of reaction green method A, B and C on reaction time and yield

	Reflux in water		Ultrasound		Microwave	
Compound	Time	Yield %	Time	Yield %	Time	Yield %
16	24 h	56%	6 min	91%	12 min	73%
17	24 h	44%	4.5 min	95%	13 min	77%
18	24 h	62%	5 min	90%	12 min	84%
19	24 h	50%	5.5 min	92%	11 min	79%
20	24 h	55%	4 min	89%	15 min	86%
21	24 h	58%	5.5 min	88%	14 min	73%
22	24 h	65%	5 min	92%	15 min	88%
23	24 h	57%	4 min	90%	12 min	84%

2.2. *In vitro* assessment

2.2.1. Agar well-diffusion zones of inhibition (ZOI). At a dosage of 5 mM, the eight novel conjugates were screened for antibacterial activity using agar well diffusion, which revealed varying antimicrobial action in opposition to the assessed bacterial and fungal organisms (Table 2). With the exception of compound **29**, every synthetic derivative was found to promote the growth of *E. coli*. ZOI ≥15 mm at a dose of 5 mM. Remarkably, hybrids **24**, **26**, **27**, **28**, **30**, and **31** displayed *E. coli* ZOI that was greater than 17.6 ± 0.33 mm, superior to that of amoxicillin. With ZOI ranging from 18 to 23 mm, *P. aeruginosa* illustrated higher sensitivity to all synthesized hybrids than to Amoxicillin (15.3 ± 0.33 mm), with the exception of the formerly described inactive hybrid **29**.

Additionally, the ZOI values of hybrids **26**, **28**, **30**, and **31** ranged from 20 to 23 mm, indicating a greater reduction in *P. aeruginosa* growth than that of Levofloxacin (19.6 ± 1.3 mm). Out of all the synthetic derivatives, hybrids **24**, **25**, **26**, and **30** showed the highest ZOI against *K. pneumoniae*, with values ranging from 17 to 21 mm, outperforming Amoxicillin (16.3 ± 0.33 mm). Only hybrid **31** showed the greatest ZOI in the case of *A. baumannii*, with a value of 17.16 ± 0.44 mm surpassing that of Amoxicillin (15.6 ± 0.33 mm), while only hybrid **28** was on par with Amoxicillin.

Nevertheless, the hybrids under investigation showed modest antibacterial efficacy against MSSA. With ZOI varying from 13 to 15 mm, all hybrids excluding **25** showed considerable antifungal efficacy against *C. albicans*, which is comparable to the common antifungal medication Fluconazole (19 ± 0.57 mm).

2.2.2. Assessment of MIC, MBC and MFC. The investigated active compounds were further tested for their minimum inhibitory concertation (MIC), minimum bactericidal concentration (MBC) and minimum fungicidal concentration (MFC). The values of the MIC, MBC, and MFC as well as the computed MBC/MIC (or MFC/MIC) ratio of the active hybrids against the aforementioned bacterial and fungal organisms, are seen in Table 3. Every synthetic chemical demonstrated broad-spectrum anti-infective activity. The strongest effect on MIC for *E. coli*, was observed upon administration of **29** with values of 6.25 μM, Verifying advantage over Levofloxacin. In MBC, the same pattern was noted, using value of 12.5 μM. Additionally, **25**, **26**, **28**, and **30** still achieved excellent MIC value of 12.5 μM against *E. coli*. Based on calculated MBC/MIC ratio (*R*), values of 2, **24**, **27**, and **29** were confirmed as bactericidal agents against *E. coli*.

Hybrids **28** and **30** displayed substantial MIC value of 6.25 μM, and MBC value of 25 μM and 50 μM, against *P. aeruginosa*, resulting in (*R*) value of 4 and 8, indicating bacteriostatic activity. Moreover, **24**, **25** and **31** displayed MIC of 12.5 μM, whereas the calculated (*R*) indicate bactericidal hybrids at higher concentrations.

In case of *K. pneumonia*, **24** and **26** displayed excellent MIC value of 12.5 μM, and a much higher MBC value resulting in a ratio above 2 indicating bacteriostatic hybrids. Compounds **28**, **29**, and **31** demonstrated moderate MIC value of 25 μM. Hybrid **28** emerged as the most potent derivative against *A. baumannii*, with MIC and MBC values of 6.25 μM and 12.5 μM, respectively, thereby identifying it as a bactericidal contender.

Table 2 ZOI diameter (mm) of the investigated hybrids, Levofloxacin, Amoxicillin and Fluconazole (at 5 mM)[a]

	Average inhibition zone diameter (mm)					
	Bacteria (Gram negative)				Bacteria (Gram positive)	Fungi
Cpd. no.	*E. coli*	*P. aeruginosa*	*K. pneumonia*	*A. baumannii*	*MSSA*	*C. albicans*
24	20.83 ± 0.60	18 ± 0.57	20.3 ± 1.2	—	—	13.8 ± 0.16
25	16.3 ± 0.33	19.6 ± 0.33	17.8 ± 0.16	—	—	—
26	19 ± 0.01	20.16 ± 0.6	20.6 ± 0.33	—	—	15 ± 0.01
27	19.3 ± 0.33	18.3 ± 0.88	15.5 ± 0.28	13.8 ± 0.16	—	14.6 ± 0.33
28	18.3 ± 0.66	22.3 ± 0.3	16.6 ± 0.33	15.5 ± 0.28	15.5 ± 0.28	13.8 ± 0.4
29	14.6 ± 0.33	14.6 ± 0.66	14 ± 0.01	13.8 ± 0.16	14.6 ± 0.66	14 ± 0.57
30	20.6 ± 0.33	21.3 ± 0.33	20.5 ± 0.28	15.3 ± 0.33	17 ± 0.01	15 ± 0.57
31	18 ± 0.57	20.6 ± 0.88	15.16 ± 0.16	17.16 ± 0.44	15.6 ± 0.33	14.6 ± 0.6
Levofloxacin	26.3 ± 0.33	19.6 ± 1.3	27.5 ± 0.28	30.5 ± 0.28	41.1 ± 0.01	NA
Amoxicillin	17.6 ± 0.33	15.3 ± 0.33	16.3 ± 0.33	15.6 ± 0.33	25 ± 0.01	NA
Fluconazole	NA	NA	NA	NA	NA	19 ± 0.57

[a] DMSO was used as a solvent with no inhibition zone.

Table 3 MIC, MBC, and MFC (μM) of the tested hybrids and calculated rate (*R*) of (MBC or MFC) toMIC

	Bacteria (Gram negative)												Bacteria (Gram positive)			Fungi		
	E.coli			*P. aeruginosa*			*K. pneumonia*			*A. baumannii*			*MSSA*			*C. albicans*		
Cpd. no.	MIC	MBC	R	MIC	MBC	R	MIC	MBC	R	MIC	MBC	R	MIC	MBC	R	MIC	MFC	R
24	25	50	2	12.5	25	2	12.5	50	4	>200	>200	—	>200	>200	—	50	100	2
25	12.5	50	4	12.5	100	8	50	200	4	>200	>200	—	>200	>200	—	12.5	50	4
26	12.5	50	4	25	50	2	12.5	50	4	>200	>200	—	>200	>200	—	50	100	2
27	25	50	2	50	100	2	50	100	2	50	50	1	>200	>200	—	50	100	2
28	12.5	50	4	6.25	25	4	25	50	2	6.25	12.5	2	12.5	25	2	100	200	2
29	6.25	12.5	2	100	200	2	25	100	4	50	100	2	6.25	12.5	2	12.5	50	4
30	12.5	50	4	6.25	50	8	50	200	4	25	50	2	25	50	2	50	100	2
31	50	200	4	12.5	50	4	25	100	4	100	100	1	6.25	25	4	100	200	2
Levofloxacin	8			4			8			2			<0.5			NA		
Amoxicillin	1			256			>1024			>1024			<0.5			NA		
Fluconazole	—			—			—			—			—			64		

Hybrids **29** and **31** displayed outstanding MIC value of 6.25 μM and MBC value of 12.5 μM and 25 μM, respectively, against MSSA. Hybrid **28**, however, demonstrated MIC and MBC values of 12.5 and 25 μM, respectively. MIC/MBC ratio confirmed hybrids **28** and **29** as bactericidal and **31** as bacteriostatic against MSSA.

With the exception of **28** and **31**, the assessed hybrids outperformed fluconazole in opposition to *C. albicans*, according to an evaluation of their fungistatic/fungicidal activities. With MBC values of 50 μM and MIC values of 12.5 μM, hybrids **25** and **29** indicated the strongest anti-fungal activity against *C. albicans*; nevertheless, the MFC to MIC Rate deemed that they were fungistatic.

2.2.3. Activity against biofilms. Since bacterial biofilm can cause a number of chronic illnesses, as was previously noted, effective therapies have become uncertain because of significant antibiotic resistance.[66,67] Therefore, we evaluated the candidate hybrids for their antibiofilm activity at sub-inhibitory concentrations to confirm that the antibiofilm activity was not due to bacteriostatic or bactericidal effect. Treatment of *P. aeruginosa* with each of the synthesized hybrids at 90% MIC resulted in 89 to 92% reduction in the production of biofilms in comparison to the untreated ones, outperforming Levofloxacin. Similar biofilm inhibition was noted upon administering 75% MIC of each assessed hybrid, excluding an outlier hybrid **31**. Examining biofilm inhibition at 50% MIC of assessed hybrids, similarly, displayed the strong biofilm inhibition, with however two outlier compounds **28** and **31** (Fig. 2).

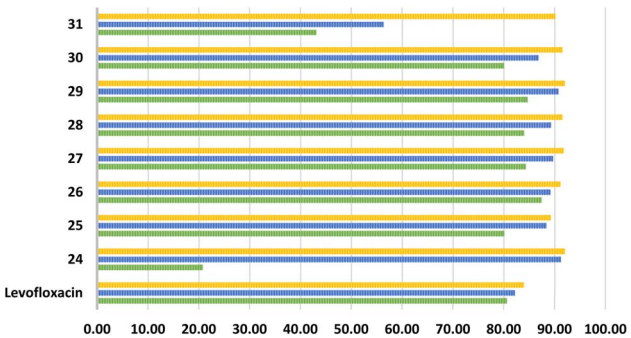

	Levofloxacin	24	25	26	27	28	29	30	31
90%MIC	83.96	91.99	89.29	91.11	91.81	91.52	91.99	91.52	90.17
75%MIC	82.20	91.30	88.42	89.17	89.75	89.34	90.81	86.87	56.38
50% MIC	80.62	20.78	80.08	87.46	84.40	83.99	84.69	80.04	43.14

% Inhibition

Fig. 2 Biofilm formation inhibition by evaluated hybrids *versus* Levofloxacin at 50%, 75% and 90% MIC.

2.2.4. Time-kill kinetics. The time-killing results of **24–31** are plotted in Fig. 3. For all eight hybrids, the killing kinetics against *P. aeruginosa* was time dependent. Higher hybrid concentrations led to a more rapid decrease in CFU number. For hybrids **24**, **26**, **27** and **29**, at 2-fold MIC, primary bacterial elimination was noticed after 3 hours, whereas bacterial elimination almost competed after 12 hours. Administering 4-fold and 8-fold MIC resulted in significant *P. aeruginosa* elimination starting at 6 hours. At 4-fold MIC of hybrids **28** and **31**, *P. aeruginosa* were almost completely killed in 24 hours, whereas primary bacterial elimination was noted at 3 hours. Administering 8-fold MIC resulted in significant *P. aeruginosa* elimination starting at 12 hours. At 8-fold MIC of hybrids **25** and **30**, all *P. aeruginosa* elimination was primarily observed after 3 hours and almost completed after 24 hours.

2.2.5. Inhibition of DNA gyrase. The potential of the novel quinoxaline hybrids to inhibit *P. aeruginosa* DNA-gyrase was assessed *in vitro* in comparison to a widely used antibiotic ciprofloxacin (Table 4). The produced compounds' IC_{50} values were expressed in-relation to ciprofloxacin, which was identified to possess a value of an IC_{50} of 143.1 μM (Fig. 4). The most effective DNA gyrase inhibitors were hybrids **25**, **28**, and **31**, with IC_{50} values that were noticeably lower than those of ciprofloxacin (77.3, 87.6, and 65.5 μM). With values of 144.7 and 147.8 μM, respectively, hybrids **26** and **30** displayed DNA gyrase inhibition analogous to that of ciprofloxacin. With IC_{50} values surpassing 150 μM, the remaining hybrids showed minimal inhibition against DNA gyrase.

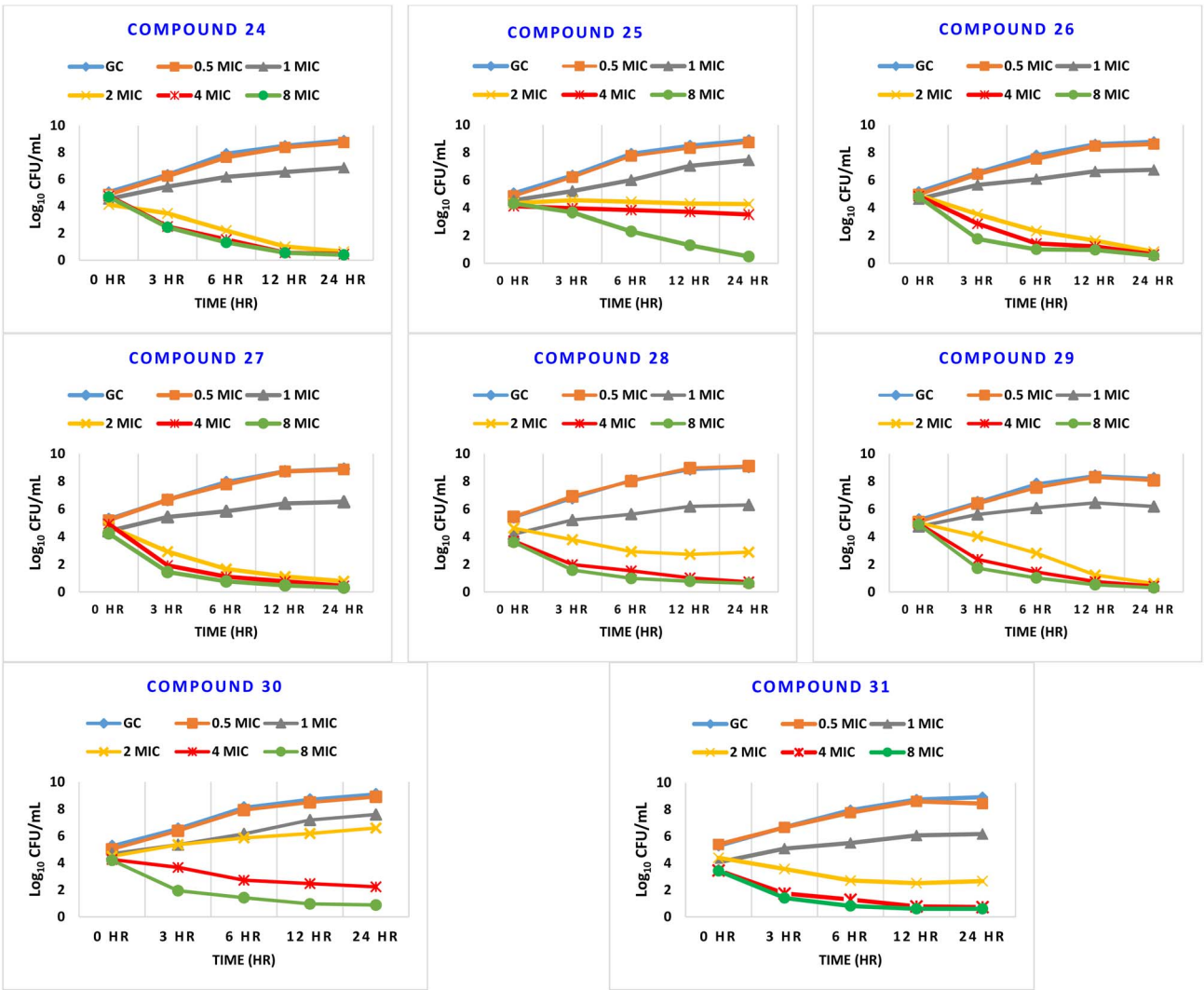

Fig. 3 Time-kill effect of **24–31** against *P. aeruginosa versus* growth control (GC).

2.3. The study of the structure–activity relationship (SAR)

This work exploited the novel compounds' biological processes to understand the connection between structure and the action (Fig. 5). The impact of the most potent chemicals on DNA Gyrase inhibitory verified that the 3-chloro-quinoxalinyl bearing hybrids are generally more active than 3-hydroxy-quinoxalinyl derivatives. Substitution on the ring of the *N*-phenyl demonstrated a pattern in the inhibitory effect of DNA gyrase, where

Table 4 DNA gyrase inhibition activity of synthesized hybrids *versus* ciprofloxacin

Cpd. no.	DNA gyrase supercoiling IC_{50} (μM)
24	172.7 ± 15.1
25	77.3 ± 15.5
26	144.7 ± 15.2
27	200.8 ± 16.4
28	87.6 ± 16.0
29	182.2 ± 16.5
30	147.8 ± 15.6
31	65.5 ± 16.8
Ciprofloxacin	143.1 ± 11.2

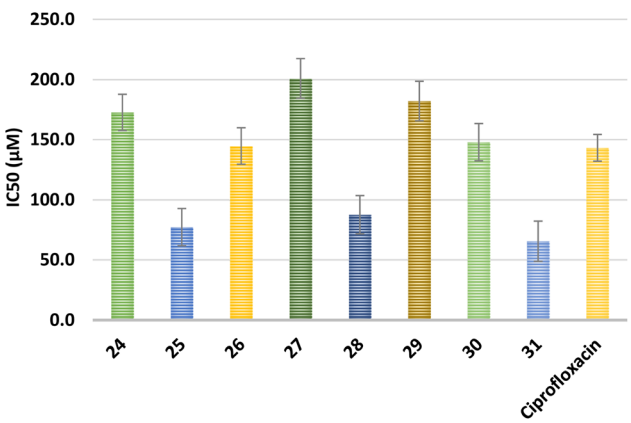

Fig. 4 The IC_{50} values of artificial hybrids on *P. aeruginosa* DNA gyrase.

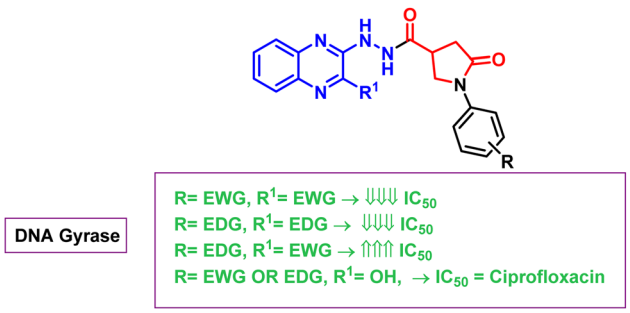

Fig. 5 SAR of pyrrolidine–quinoxaline hybrids.

electron-withdrawing groups on the *para* position demonstrated superior activity to Ciprofloxacin as observed with **28** and **31**. The remaining 3-chloro-quinoxalinyl hybrids bearing electron-donating groups on the *N*-phenyl ring (**30**) and (**29**) demonstrated DNA gyrase inhibitory activity either equipotent or lower than Ciprofloxacin, respectively. This finding confirms the importance of bearing electron-withdrawing groups at both R and R^1. Most importantly, Presence of 3-hydroxy substitution on the *N*-phenyl ring generally resulted in lower DNA gyrase inhibitory activity, however equipotent to Ciprofloxacin. Such a trend was not noted in hybrid **26**, bearing two hydroxyl groups. A plausible explanation for this exception suggests the formation of an extra compensatory hydrogen bond with DNA gyrase. It was noted, however that hybrids bearing both R groups as electron-donating still exhibited equipotent or superior DNA gyrase inhibitory activity to Ciprofloxacin (hybrids **26** and **25**, respectively).

2.4. *In silico* ADME

To assess the physicochemical characteristics of the produced hybrids in comparison to levofloxacin, amoxicillin, and fluconazole, a simulated study was conducted.[68–70] In terms of their physicochemical characteristics, all compounds and reference drugs—aside from **27**—display zero breaches of the Lipinski's requirements regarding oral medications, as stated by Table 5. With the exception of **27** and amoxicillin, all examined derivatives and references adhere to Veber's requirements.

Table 6 TPSA and %ABS of the synthesized differences

Cpd. no.	TPSA	% ABS
24	131.240	63.720
25	107.450	71.920
26	127.680	64.950
27	153.270	56.120
28	111.010	70.700
29	87.220	78.900
30	107.450	71.920
31	133.040	63.100
Levofloxacin	84.240	79.180
Amoxicillin	158.260	52.980
Fluconazole	81.650	80.090
Ciprofloxacin	74.570	82.600

Additionally, all hybrids exhibit high flexibility with no more than six rotatable bonds. This implies that oral consumption of the eight hybrids is possible. Each analogue was given a score between 3.05 and 3.76 for ease of manufacturing, suggesting that a large number of them can be produced on a large scale.

Additionally, the percentage was computed using TPSA as follows: % ABS = 109 − (0.354 × TPSA).[71,72] All of the prospective antibacterial agents possess estimated absorption percentages between 87 and 154%, which indicates strong oral bioavailability analogous to reference medications. The percentage of ABS ranges from 56 to 79% (Table 6).

The findings of monitoring the new antibacterial hybrids for pharmacokinetic and medicinal chemistry characteristics suggest that, with the exception of **27** and amoxicillin, every other compound has demonstrated adequate GI tract absorption. They can't overcome all, however, overcome the brain–blood barrier. Every hybrid has a high probability of effluxing outside the cell and is a P-gp (P-glycoprotein) substrate.

Furthermore, inhibition of metabolic enzymes by investigated hybrids was computationally assessed. Predictions revealed that hybrid **26** did not inhibit any of the assessed metabolic enzymes, whereas **27** only inhibited CYP2C9.

All investigated hybrids received a bioavailability score of 0.55, with the exception of derivative **24**, which received a score of 0.56, analogous to the other reference drugs. We assessed every hit, and PAINS showed no warnings. In order to avoid

Table 5 Physicochemical characteristics of the most physiologically active drugs compared to reference medications

Cpd. no.	HBD	HBA	MW	*M* log *P*	No. of rotatable bonds	Lipinski's violations	Veber's violations	Synthetic accessibility
24	3	6	388.38	1.09	5	0	0	3.64
25	3	5	391.42	2.16	5	0	0	3.76
26	4	6	379.37	1.2	5	0	0	3.67
27	3	7	408.37	0.88	6	1	1	3.71
28	2	5	406.83	1.68	5	0	0	3.05
29	2	4	409.87	2.76	5	0	0	3.31
30	3	5	397.82	1.8	5	0	0	3.30
31	2	6	426.81	1.47	6	0	0	3.49
Levofloxacin	2	7	379.38	0.2	2	0	0	3.74
Amoxicillin	4	6	365.40	0.23	5	0	1	4.17
Fluconazole	1	7	306.27	1.47	5	0	0	2.45
Ciprofloxacin	2	5	331.34	1.28	3	0	0	2.51

Table 7 Medicinal chemistry parameters and pharmacokinetic features

Cpd. no.	GI absorption	BBB permeation	Pgp substrate	CYP1A2 inhibitor	CYP2C19 inhibitor	CYP2C9 inhibitor	CYP2D6 inhibitor	CYP3A4 inhibitor	Bioavailability score	PAINS alerts
24	High	No	Yes	Yes	No	Yes	No	No	0.56	0
25	High	No	Yes	Yes	No	Yes	Yes	Yes	0.55	0
26	High	No	Yes	No	No	No	No	No	0.55	0
27	Low	No	Yes	No	No	Yes	No	No	0.55	0
28	High	No	Yes	Yes	No	Yes	Yes	Yes	0.55	0
29	High	No	Yes	Yes	Yes	Yes	Yes	Yes	0.55	0
30	High	No	Yes	Yes	No	Yes	Yes	Yes	0.55	0
31	High	No	Yes	No	Yes	Yes	No	Yes	0.55	0
Levofloxacin	High	No	Yes	No	No	No	No	No	0.55	0
Amoxicillin	Low	No	No	No	No	No	No	No	0.55	0
Fluconazole	High	No	Yes	No	Yes	No	No	No	0.55	0
Ciprofloxacin	High	No	Yes	No	No	No	No	No	0.55	0

inaccurate outcomes, PAINS are important considerations while developing drugs (Table 7). The evaluated substances' bioavailability radar is illustrated within Fig. 6. The intended hybrids revealed promise as attractive agents for antibacterial treatment by exhibiting typically very good physicochemical properties.

2.5. Toxicity assessment *in silico*

The pkCSM online tools confirm the security of the most active hits since, as shown in Table 8, with the exception of **31**, none have demonstrated the potential for mutagenicity according to AMES toxicity, equivalent to that of Levofloxacin and Fluconazole. Furthermore, compared to Fluconazole (0.114 log mg per kg per day) and other hits, hybrid **26** demonstrated a maximum acceptable human dose of 0.261 log mg per kg per day. The LD_{50} value of compound **31** has been estimated to be 2.587 mol kg^{-1}, which is considerably higher than that of Fluconazole and equivalent to that of Levofloxacin. Additionally, compound **26** had an LOAEL value of 2.798 log mg per kg bw per day, surpassing the values of all hits and the reference drugs. The potassium channels encoded by the hERG gene control the repolarization of cardiac action potentials. Pharmaceutical companies are concerned because blocking. These channels may cause cardiovascular problems that could be fatal. While every potent ingredient was expected to have an inhibitory impact on hERG-II, it was shown that they had no effect on hERG-I.

The pkCSM server was used to examine hepatotoxicity. All active hits, including reference medications, were predicted to be hepatotoxic. Skin discomfort was not evident in any of the hits. It was expected that Levofloxacin, Fluconazole, and active hybrids would be categorized as a class IV (GHS) utilizing the-ProTox-II identification webtool (Table 8). It was discovered that all active hybrids had LD_{50} values exceeding the reference medications. None of the active hits were supposed to be immunotoxic, cytotoxic, or mutagenic. The active hybrids and reference drugs were expected to exhibit both neurotoxicity and clinical toxicity. Neither the voltage-gated sodium channel (VGSC) nor the phosphoprotein (tumor suppressor) p53 were suppressed by those active hybrids.

2.6. Molecular docking

The investigated hybrids were docked against DNA gyrase (PDB ID: 8BN6) to predict binding mode and interactions. The bound ligand was separately redocked to validate the docking procedure Validation was confirmed by visualizing the overlay of the original and the redocked pose (Fig. 7) and calculated RMSD value of 0.79 Å. The investigated hybrids were docked implementing the same parameters. The 2D interactions and energy scores are recorded (Table 9).

The interaction of co-crystalized ligand with DNA Gyrase involved six alkyl-type van der Waals interactions with Val73, Val169, Val45 and Val122. Two H-bonds were noted between the co-crystalized ligand and key amino acids: Arg138 and Thr167. Three pi–alkyl interactions were observed with Pro81 and Ile96. Glu52 interacted with the ligand through two pi–anion interactions, whereas Arg78 interacted through one pi–cation interactions. Amide-pi stacked interaction was involved with Asn48.

Docking of ciprofloxacin as a reference against DNA Gyrase demonstrated that the binding energy was −9.70 kcal per mol. Ciprofloxacin was able to interact with key amino acids; including three H-bonds with The167, Arg138 and Arg78, two alkyl-type van der Waals interactions with Ile96 and Ile80, one pi–alkyl interaction with Ile80, one amide–pi stacked interaction with Asn48, and two pi–anion interactions with Glu52.

Simulation of the hybrid **25** binding showed that the binding energy was −8.12 kcal mol^{-1}. Key amino acids were involved in the interaction of **25** with DNA Gyrase. Such interactions included two amide-Pi stacked interactions with Asn48, two pi–alkyl-type van der Waals interactions with Ile96 and Val122, one H-bond with Thr167 and one alkyl-type van der Waals with Ile96. Additional interactions included two pi–alkyl interactions with Ile80, two H-bonds with Asp75 and one amide–pi stacked interaction with Gly79.

Binding simulation of hybrid **28** demonstrated a binding energy of −8.05 kcal mol^{-1}. Key amino acids were involved in the interaction of **28** with DNA Gyrase. Such interactions included two pi-alkyl-type van der Waals interactions with Ile96, one H-bond with Val122. Additional interactions involved two pi–alkyl interactions with Ile 80, and one amide–pi stacked interaction with Gly79.

Fig. 6 The bioavailability radar of the assessed hybrids and the drugs that are referenced are correlated. The area that is colored provides ideal chemical and physical conditions for absorption through the mouth. Insolubility (INSOLU), unsaturation (INSATU), polarity (POLAR), molecular weight (SIZE), lipophilicity (LIPO), and flexibility (FLEX).

Binding simulation of hybrid **31** revealed that the binding energy score was −10.80 kcal mol^{-1}. Although docking scores do not strictly follow experimental IC_{50} values, the binding energy of **31** still confirms superiority to Ciprofloxacin *in silico*. Key amino acids were involved in the interaction of **31** with DNA Gyrase. Such interactions included three pi–alkyl-type van der Waals interactions with Val169, Val122 and Ile96, one H-bond with Glu52, and two amide–pi stacked interactions with Asn48. Additional interactions involved two pi–alkyl interactions with Ile80.

The binding mode and energies of the remaining hybrids are noted in (Table 9, Fig. 8 and 9).

3. Experimental

3.1. Chemistry

3.1.1. Synthesis of 16–23

3.1.1.1 Method A. In a flask with a round bottom, 1 mmol (0.13 g) of itaconic acid (**1**) was mixed with 1 mmol of each of the respective amines **8–15** with water. The mixture of the reaction

Table 8 Toxicity of the most active hybrids **25**, **26**, **30**, and **31** *versus* with Levofloxacin and Fluconzaole

	Most active compounds					
Test	**25**	**26**	**30**	**31**	**Levofloxacin**	**Fluconazole**
pkCSM[73]						
AMES toxicity	No	No	No	Yes	No	No
Max. tolerated dose (human)	−0.11	0.261	0.144	0.021	0.965	0.114
hERG I inhibitor	No	No	No	No	No	No
hERG II inhibitor	Yes	Yes	Yes	Yes	No	No
Oral rat acute toxicity (LD_{50})	2.046	2.089	2.116	2.587	2.59	2.328
Oral rat chronic toxicity (LOAEL)	1.504	2.798	2.046	2.07	1.791	1.033
Hepatotoxicity	Yes	Yes	Yes	Yes	Yes	Yes
Skin sensitization	No	No	No	No	No	No
T. Pyriformis toxicity	0.405	0.346	0.357	0.326	0.285	0.312
Minnow toxicity	0.812	1.777	0.187	−0.601	1.273	3.872
ProTox-II prediction[74]						
LD_{50} (mg kg^{-1})	2000	1600	1600	2000	1478	1271
Toxicity class	IV	IV	IV	IV	IV	IV
Neurotoxicity	+(0.72	+(0.73)	+(0.9)	+(0.57)	+(0.93)	+(0.91)
Nephrotoxicity	−(0.53)	−(0.53)	+(0.58)	−(0.54)	+(0.85)	−(0.61)
Immunotoxicity	−(0.99)	−(0.98)	−(0.96)	−(0.98)	−(0.99)	−(0.83)
Mutagenicity	−(0.57)	−(0.58)	−(0.54)	+(0.79)	+0.66)	−(0.52)
Cytotoxicity	−(0.57)	−(0.6)	−(0.6)	−(0.53)	−(0.69)	−(0.76)
Clinical toxicity	+(0.66)	+(0.68)	+(0.73)	+(0.58)	+(0.62)	+(0.55)
Phosphoprotein (tumor suppressor) p53	−(0.88)	−(0.88)	−(0.87)	−(0.86)	−(0.98)	−(0.97)
Voltage gated sodium channel (VGSC)	−(0.89)	−(0.76)	−(0.7)	−(0.82)	−(0.95)	−(0.95)

underwent reflux heating for 24 hours. The resulting precipitates were filtered recrystallized from ethanol.[75–78]

3.1.1.2 Method B. In a beaker of 250 mL, 1 mmol (0.13 g) itaconic acid (**1**) was dissolved in the least amount of ethanol and mixed with 1 mmol of each of the respective amines **8–15**. The reaction solution was sonicated until reaction completion, monitored by TLC.

3.1.1.3 Method C. In a 250 mL beaker, 1 mmol (0.13 g) itaconic acid (**1**) was dissolved in the least amount of ethanol and mixed with 1 mmol of each of the respective amines **8–15**. The reaction solution was microwaved in domestic microwave until reaction completion, monitored by TLC.

*3.1.1.4 1-(3-Chlorophenyl)-5-oxopyrrolidine-3-carboxylic acid, **8**.* Yellowish powder; yield: 91%, m.p. 187–189 °C; ^{1}H NMR (400 MHz, $CDCl_3$): δ = 12.38 (s, 1H, COOH), 7.28–7.24 (m, 3H, A–H), 7.20–7.15 (m, 1H, A–H), 4.19 (dd, J = 11.9, 4.4 Hz, 1H, pyrrolidine CH_2), 3.93 (dd, J = 11.9, 4.4 Hz, 1H, pyrrolidine CH_2), 3.33–3.24 (m, 1H, pyrrolidine CH), 2.78 (dd, J = 15.0, 5.6 Hz, 1H, pyrrolidine CH_2), 2.53 (dd, J = 15.0,5.6 Hz, 1H, pyrrolidine CH_2).

*3.1.1.5 1-(4-Chlorophenyl)-5-oxopyrrolidine-3-carboxylic acid, **9**.* Yellowish powder; yield: 95%, m.p. 184–185 °C; ^{1}H NMR (400 MHz, $CDCl_3$): δ = 12.14 (s, 1H, COOH), 7.31–7.22 (m, 2H, A–H), 7.08–7.00 (m, 2H, A–H), 4.15 (dd, J = 11.8, 4.5 Hz, 1H, pyrrolidine CH_2), 3.90 (dd, J = 11.8, 4.2 Hz, 1H, pyrrolidine CH_2), 3.37–3.27 (m, 1H, pyrrolidine CH), 2.76 (dd, J = 14.9, 5.5 Hz, 1H, pyrrolidine CH_2), 2.51 (dd, J = 14.9,5.5 Hz, 1H, pyrrolidine CH_2).

*3.1.1.6 1-(4-Cyanophenyl)-5-oxopyrrolidine-3-carboxylic acid, **10**.* Orange powder; yield: 90%, m.p. 181–183 °C; ^{1}H NMR (400 MHz,$CDCl_3$): δ = 12.38 (s, 1H, COOH), 7.58 (d, J = 7.5 Hz, 2H, A–H), 7.30 (d, J = 7.1 Hz, 2H, A–H), 4.17 (dd, J = 11.7, 4.2 Hz, 1H, pyrrolidine CH_2), 3.92 (dd, J = 12.0,4.4 Hz, 1H, pyrrolidine CH_2), 3.29 (p, J = 4.9 Hz, 1H, pyrrolidine CH), 2.78 (dd, J = 14.8,5.6 Hz, 1H, pyrrolidine CH_2), 2.53 (dd, J = 14.8,5.6 Hz, 1H, pyrrolidine CH_2).

*3.1.1.7 1-(2,5-Dimethylphenyl)-5-oxopyrrolidine-3-carboxylic acid, **11**.* Ligh yellow powder; yield: 92%, m.p. 196–198 °C; ^{1}H NMR (400 MHz, $CDCl_3$): δ = 12.13 (s, 1H, COOH), 6.97 (d, J = 2.8 Hz, 1H, A–H), 6.87 (d, J = 8.5 Hz, 1H, A–H), 6.72 (dd, J = 8.6,2.9 Hz, 1H, A–H), 4.32 (dd, J = 11.6, 4.3 Hz, 1H, pyrrolidine CH_2), 4.07 (dd, J = 11.6, 4.3 Hz, 1H, pyrrolidine CH_2), 3.04–2.93 (m, 1H, pyrrolidine CH), 2.70 (dd, J = 15.0, 5.6 Hz, 1H, pyrrolidine CH_2), 2.44 (dd, J = 14.9, 5.6 Hz, 1H, pyrrolidine CH_2), 2.17 (s, 3H, CH_3), 2.09 (s, 3H, CH_3).

*3.1.1.8 1-(3-Hydroxyphenyl)-5-oxopyrrolidine-3-carboxylic acid, **12**.* Yellowish powder; yield: 89%, m.p. 179–181 °C; ^{1}H NMR (400 MHz,$CDCl_3$): δ = 12.38 (s, 1H, COOH), 7.98 (s, 1H, OH), 7.11 (t, J = 7.9 Hz, 1H, A–H), 7.02 (d, J = 7.1 Hz, 1H, A–H), 6.65 (d, J = 8.3 Hz, 1H, A–H), 6.59 (d, J = 2.6 Hz, 1H, A–H), 4.19 (dd, J = 11.9, 4.3 Hz, 1H, pyrrolidine CH_2), 3.93 (dd, J = 11.9, 4.4 Hz, 1H, pyrrolidine CH_2), 3.29 (p, J = 4.8 Hz, 1H, pyrrolidine CH), 2.78 (dd, J = 15.0, 5.4 Hz, 1H, pyrrolidine CH_2), 2.53 (dd, J = 15.1, 5.6 Hz, 1H, pyrrolidine CH_2).

*3.1.1.9 1-(4-Nitrophenyl)-5-oxopyrrolidine-3-carboxylic acid, **13**.* Orange powder; yield: 88%, m.p. 198–200 °C; ^{1}H NMR (400 MHz, $CDCl_3$): δ = 13.14 (s, 1H, COOH), 8.05 (d, J = 7.2 Hz, 2H, A–H), 7.43 (d, J = 7.4 Hz, 2H, A–H), 3.98 (dd, J = 11.9, 4.4 Hz, 1H, pyrrolidine CH_2), 3.73 (dd, J = 11.8, 4.3 Hz, 1H, pyrrolidine CH_2), 3.38 (p, J = 4.8 Hz, 1H, pyrrolidine CH), 2.79 (dd, J = 14.9,

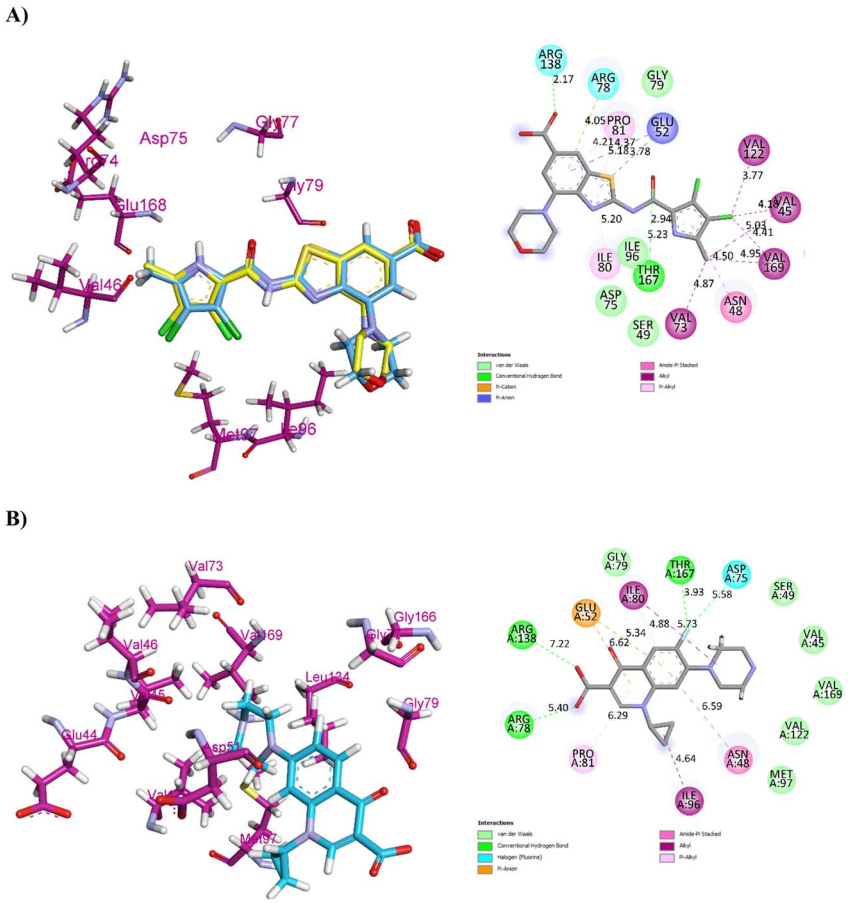

Fig. 7 (A) Overlay of bound ligand (cyan) and redocked ligand (yellow) and bound ligand interactions, (B) binding mode and ligand interactions of Ciprofloxacin.

5.6 Hz, 1H, pyrrolidine CH_2), 2.54 (dd, J = 14.8, 5.6 Hz, 1H, pyrrolidine CH_2).

3.1.1.10 1-(Naphthalen-1-yl)-5-oxopyrrolidine-3-carboxylic acid, ***14****.* Light yellow powder; yield: 92%, m.p. 195–196 °C; ^{1}H NMR (400 MHz, $CDCl_3$): δ = 12.13 (s, 1H, COOH), 7.78–7.64 (m, 3H, A–H), 7.42–7.22 (m, 3H, A–H), 7.14 (d, J = 7.8 Hz, 1H, A–H), 4.32 (dd, J = 11.5, 4.3 Hz, 1H, pyrrolidine CH_2), 4.06 (dd, J = 11.6, 4.4 Hz, 1H, pyrrolidine CH_2), 2.99 (p, J = 4.6 Hz, 1H, pyrrolidine CH), 2.70 (dd, J = 15.0, 5.7 Hz, 1H, pyrrolidine CH_2), 2.45 (dd, J = 15.0, 5.6 Hz, 1H, pyrrolidine CH_2).

3.1.1.11 5-Oxo-1-phenylpyrrolidine-3-carboxylic acid, ***15****.* Yellow powder; yield: 90%, m. p. 186–187 °C; ^{1}H NMR (400 MHz,$CDCl_3$): δ = 12.38 (s, 1H, COOH), 7.36–7.15 (m, 5H, A–H), 4.17 (dd, J = 11.9, 4.2 Hz, 1H, pyrrolidine CH_2), 3.92 (dd, J = 11.9, 4.4 Hz, 1H, pyrrolidine CH_2), 3.33–3.24 (m, 1H, pyrrolidine CH), 2.78 (dd, J = 15.0, 5.6 Hz, 1H, pyrrolidine CH_2), 2.53 (dd, J = 15.0, 5.6 Hz, 1H, pyrrolidine CH_2).

3.1.2. Synthesis of hybrids 24–31. In a 250 mL beaker, 1 mmol of 2-hydroxy-3-hydrazinylquinoxaline (**4**) (0.17 g) or 2-chloro-3-hydrazinylquinoxaline (**6**) (0.19 g) was dissolved in the least amount of ethanol with 1 mmol of each of fragments **18–21**. The reaction solution was sonicated until reaction completion monitored by TLC.[79–83]

3.1.2.1 1-(4-Cyanophenyl)-N′-(3-hydroxyquinoxalin-2-yl)-5-oxopyrrolidine-3-carbohydrazide, ***24****.* Orange powder; yield: (59%), m.p. 264–265 °C; IR (KBr, cm^{-1}) = 3474–3359 (2NH & OH), 3073 (CH aromatic), 2214 (CN), 1687 (br. 2C=O); ^{1}H NMR (400 MHz, $CDCl_3$): δ = 12.87 (s, 1H, OH), 11.04 (d, J = 6.6 Hz, 1H, –NH–**NH**–CO), 8.18 (d, J = 6.8 Hz, 1H, **NH**–NH–CO), 8.05 (dd, J = 7.7, 2.0 Hz, 1H, A–H), 7.73–7.52 (m, 5H, A–H), 7.30 (d, J = 7.8 Hz, 2H, A–H), 4.17 (dd, J = 12.4, 3.6 Hz, 1H, pyrrolidine CH_2), 3.92 (dd, J = 12.5, 3.5 Hz, 1H, pyrrolidine CH_2), 3.12 (m, 1H, pyrrolidine CH), 2.52 (dd, J = 15.7, 4.9 Hz, 1H, pyrrolidine CH_2), 2.33 (dd, J = 15.6, 4.9 Hz, 1H, pyrrolidine CH_2); ^{13}C NMR (100 MHz,$CDCl_3$): δ = 172.77 (C=O), 171.24 (C=O), 146.52, 141.54, 140.22, 136.97, 136.51, 132.41, 128.93, 126.45, 125.38, 123.42, 118.23 (CN), 117.28, 102.21, 48.51 (pyrrolidine **C**H_2), 38.02 (pyrrolidine **C**H), 36.42 (pyrrolidine **C**H_2); MS(EI, 70 eV): m/z (%) = 388 [$M^{+\cdot}$] (18%), 356.46 (100%); anal. calc. for: $C_{20}H_{16}N_6O_3$ (388.38): C, 61.85; H, 4.15; N, 21.64; found: C, 61.80; H, 4.17; N, 21.68.

3.1.2.2 1-(2,5-Dimethylphenyl)-N′-(3-hydroxyquinoxalin-2-yl)-5-oxopyrrolidine-3-carbohydrazide, ***25****.* Light brown powder; yield: (77%), m.p. 271–272 °C; IR (KBr, cm^{-1}) = 3369–3280 (br. 2NH & OH), 3060 (CH aromatic), 2971, 2860 (CH aliphatic), 1698 (br. 2C=O; ^{1}H NMR (400 MHz,$CDCl_3$): δ = 12.86 (s, 1H, OH), 10.79 (d, J = 6.8 Hz, 1H, –NH–**NH**–CO), 8.88 (d, J = 6.6 Hz, 1H,

Table 9 Binding energies and interactions of bound ligand and hybrids against DNA Gyrase (PDB: 8BN6)

Cpd. no.	S (kcal mol^{-1})	Type of interaction	Amino acid	Length (Å)	Cpd. no.	S (kcal mol^{-1})	Type of interaction	Amino acid	Length (Å)
24	−8.35	Amide–Pi stacked	Asn48	5.01	**28**	−8.05	Pi–alkyl	Ile80	4.44
		Amide–Pi stacked	Asn48	4.66			Pi–alkyl	Ile80	4.51
		Pi–alkyl	Ile80	4.41			Amide–Pi stacked	Gly79	4.50
		Pi–alkyl	Ile80	4.40			H-bond	Val122	4.85
		H-bond	Thr167	2.17			Pi–alkyl	Ile96	5.55
		H-bond	Asp75	1.97			Pi–alkyl	Ile96	7.25
		Amide–Pi stacked	Gly79	5.10					
		Pi–alkyl	Ile96	4.78					
		Pi–alkyl	Val122	5.35					
		H-bond	Arg138	2.96					
25	−8.12	Amide–Pi stacked	Asn48	4.64	**29**	−7.66	Alkyl	Ile96	5.35
		Amide–Pi stacked	Asn48	5.00			Alkyl	Pro81	4.41
		Pi–alkyl	Ile80	4.41			H-bond	Arg138	2.82
		Pi–alkyl	Ile80	4.44			Pi–alkyl	Ile80	4.25
		H-bond	Asp75	1.95			Pi–alkyl	Ile80	4.23
		H-bond	Asp75	3.12			Amide–Pi stacked	Gly79	4.80
		Amide–Pi stacked	Gly79	5.12					
		Pi–alkyl	Ile96	4.46					
		Alkyl	Ile96	4.52					
		H-bond	Thr167	2.16					
		Pi–alkyl	Val122	5.32					
26	−7.81	H-bond	Arg138	2.23	**30**	−10.20	H-bond	Asp51	1.96
		H-bond	Asp75	2.79			Amide–Pi stacked	Asn48	5.07
		H-bond	Gly79	2.27			Amide–Pi stacked	Asn48	4.69
		Amide–Pi-stacked	Gly79	4.36			Pi–alkyl	Val122	5.25
		Pi–alkyl	Ile80	4.10			Pi–alkyl	Val169	5.43
		Pi–alkyl	Ile80	4.37			Pi–alkyl	Ile80	5.32
		H-bond	Glu52	2.85			Pi–alkyl	Ile80	4.29
27	−7.41	Pi–alkyl	ILE96	4.48	**31**	−10.80	H-bond	GLU52	3.07
		Pi–alkyl	VAL122	5.34			Pi–alkyl	ILE80	4.34
		H-bond	ARG138	3.06			Pi–alkyl	ILE80	5.42
		Amide Pi-stacked	ASN48	4.99			Pi–alkyl	VAL169	5.35
		Amide Pi-stacked	ASN48	4.65			Amide Pi-stacked	ASN48	5.08
		Pi–alkyl	ILE80	4.43			Amide Pi-stacked	ASN48	4.65
		Pi–alkyl	ILE80	4.41			Pi–alkyl	VAL122	5.22
		H-bond	ASP75	3.12			Pi–alkyl	ILE96	4.66
		H-bond	ASP75	1.95					
		Amide Pi-stacked	GLY79	5.11					
		H-bond	THR167	2.16					
Co-crystalized	−9.34	H-bond	ARG138	2.17	**Ciprofloxacin**	−9.70	H-bond	ARG138	7.22
		Pi–cation	ARG78	4.05			Pi–anion	GLU52	6.62
		Pi–alkyl	PRO81	4.21			Pi–anion	GLU52	5.34
		Pi–alkyl	PRO81	4.37			Pi–alkyl	ILE80	4.88
		Pi–anion	GLU52	5.18			Alkyl	ILE80	5.73
		Pi–anion	GLU52	3.78			H-bond	THR167	3.93
		Pi–alkyl	ILE96	5.23			Halogen	ASP75	5.58
		H-bond	THR167	2.94			Amide–pi stacked	ASN48	6.59
		Alkyl	VAL73	4.87			Alkyl	ILE96	4.64
		Amide–Pi stacked	ASN48	4.50			H-bond	ARG78	5.40
		Alkyl	VAL169	4.95					
		Alkyl	VAL169	4.41					
		Alkyl	VAL45	5.03					
		Alkyl	VAL45	4.18					
		Alkyl	VAL122	3.77					

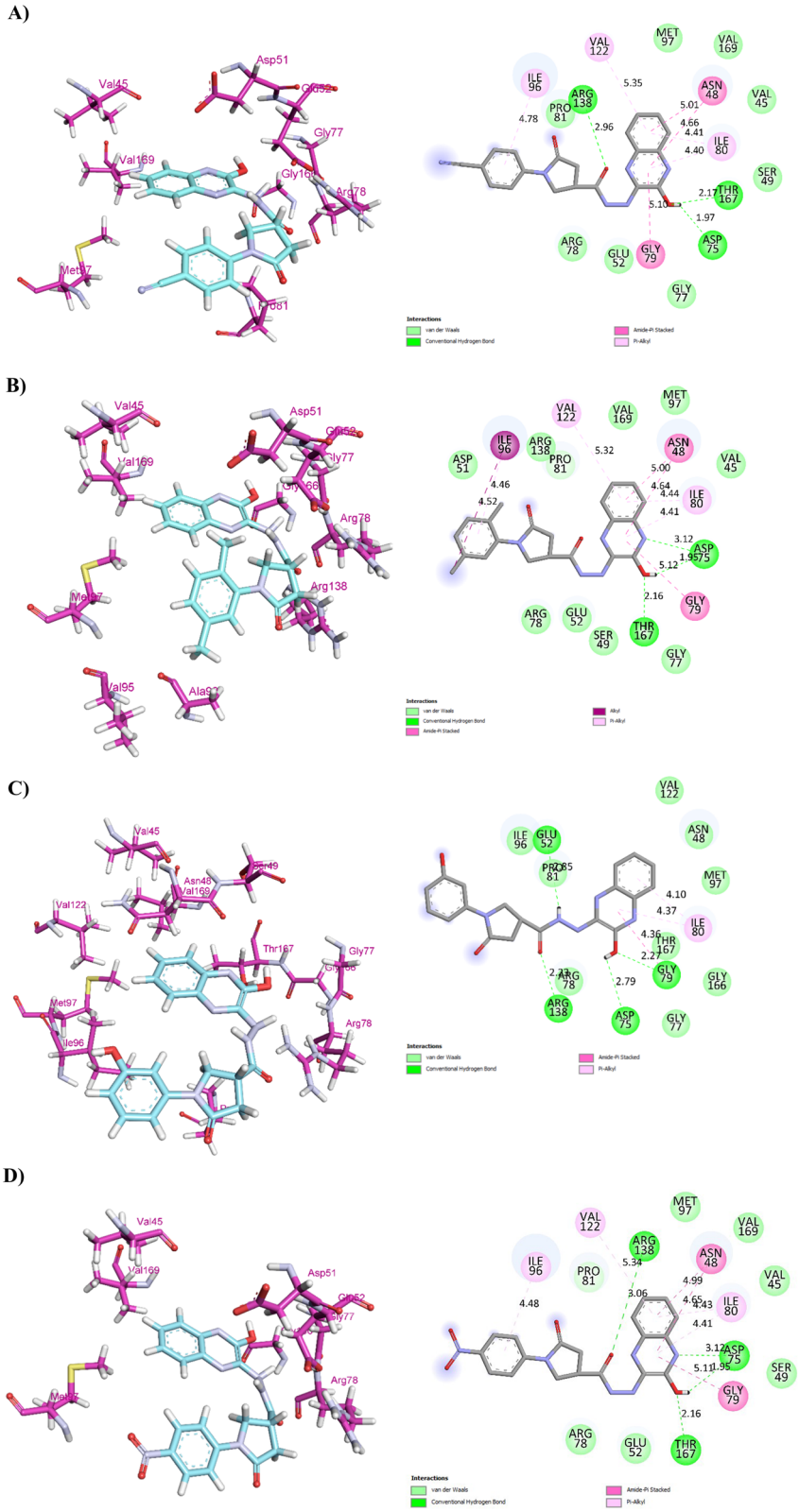

Fig. 8 Binding mode and ligand interactions of (A) 24 (B) 25 (C) 26 (D) 27.

NH–NH–CO), 7.91 (dd, J = 8.0, 1.6 Hz, 1H, A–H), 7.68 (dd, J = 8.0, 1.8 Hz, 1H, A–H), 7.65–7.52 (m, 2H, A–H), 7.12 (d, J = 8.2 Hz, 1H, A–H), 6.98 (d, J = 8.2 Hz, 2H, A–H), 4.21 (dd, J = 12.2, 3.6 Hz, 1H, pyrrolidine CH_2), 3.96 (dd, J = 12.3, 3.7 Hz, 1H, pyrrolidine CH_2), 3.34–3.25 (m, 1H, pyrrolidine CH), 2.75 (dd, J = 15.7, 4.9 Hz, 1H, pyrrolidine CH_2), 2.53 (dd, J = 15.7, 4.9 Hz, 1H,

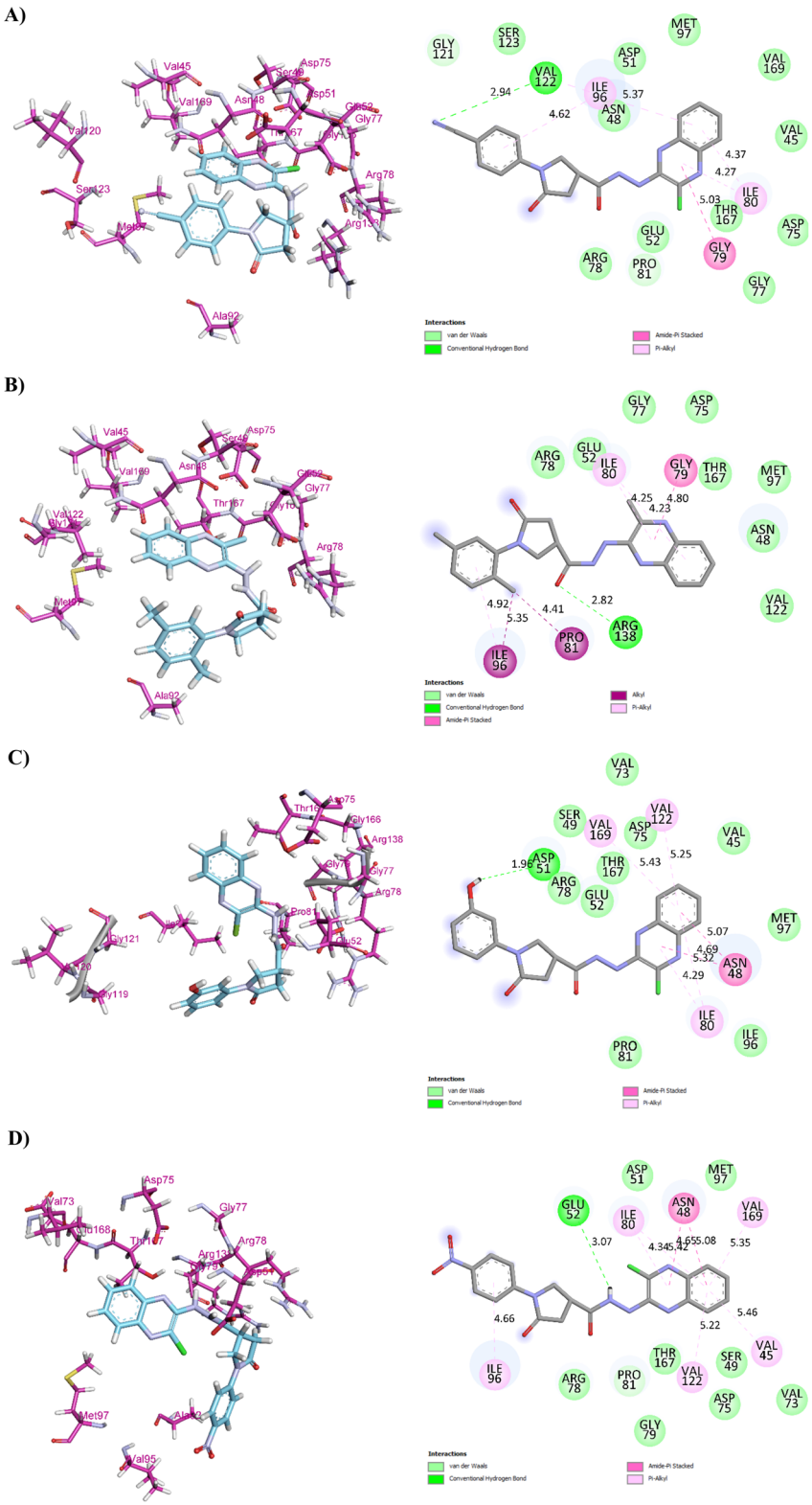

Fig. 9 The ligand interactions and binding mechanism of (A) 28 (B) 29 (C) 30 (D) 31.

pyrrolidine CH_2), 2.28 (s, 3H, CH_3), 2.10 (s, 3H, CH_3); ^{13}C NMR (100 MHz,$CDCl_3$): δ = 172.15 (C═O), 171.54 (C═O), 145.99, 140.73, 137.35, 136.84, 135.02, 132.42, 129.63, 129.36, 129.05, 126.42, 125.73, 123.93, 123.84, 121.82, 49.31 (pyrrolidine CH_2), 38.12 (pyrrolidine CH), 36.32 (pyrrolidine CH_2), 19.52 (CH_3), 16.53 (CH_3); MS (EI, 70 eV): m/z (%) = 391.94 [$M^{\cdot+}$] (16.89%), 74.07 (100%); anal. calc. for: $C_{21}H_{21}N_5O_3$ (391.42): C, 64.44; H, 5.41; N, 17.89; found: C, 64.48; H, 5.38; N, 17.85.

*3.1.2.3 1-(3-Hydroxyphenyl)-N′-(3-hydroxyquinoxalin-2-yl)-5-oxopyrrolidine-3-carbohydrazide, **26**.* Dark yellow powder; yield: (62%), m.p. 243–244 °C; IR (KBr, cm^{-1}) = 3422–3269 (br. 2NH & 2OH), 3070 (CH aromatic), 1656–1703 (br. 2C═O; ^{1}H NMR (400 MHz,$CDCl_3$): δ = 11.03 (s, 1H, OH), 8.80 (d, J = 6.6 Hz, 1H, –NH–**NH**–CO), 8.60 (s, 1H, OH), 8.17 (d, J = 8.1 Hz, 1H, A–H), 7.73 (dd, J = 8.1, 1.6 Hz, 1H, 1H, A–H), 7.70–7.54 (m, 2H, 1H, A–H), 7.09 (t, J = 7.9 Hz, 1H, 1H, A–H), 6.83 (d, J = 6.9 Hz, 1H, A–H), 6.68 (d, J = 8.6 Hz, 1H, A–H), 6.54 (t, J = 2.3 Hz, 1H), 5.90 (d, J = 6.8 Hz, 1H, –**NH**–NH–CO), 3.90 (dd, J = 12.5, 3.5 Hz, 1H, pyrrolidine **C**H_2), 3.65 (dd, J = 12.5, 3.7 Hz, 1H, pyrrolidine **C**H_2), 3.08–3.00 (m, 1H, pyrrolidine **C**H), 2.54 (dd, J = 15.6, 4.9 Hz, 1H, pyrrolidine **C**H_2), 2.40 (dd, J = 15.8, 4.8 Hz, 1H, pyrrolidine **C**H_2); ^{13}C NMR (100 MHz,$CDCl_3$): δ = 173.48 (C═O), 172.48 (C═O), 158.81, 147.23, 147.07, 140.85, 136.93, 135.59, 131.70, 131.16, 129.32, 125.08, 122.44, 117.35, 109.00, 106.54, 49.02 (pyrrolidine **C**H_2), 40.83 (pyrrolidine **C**H), 38.00 (pyrrolidine **C**H_2); MS (EI, 70 eV): m/z (%) = 379.40 [$M^{\bullet+}$] (19.76%), 190.16 (100%); anal. calc. for: $C_{19}H_{17}N_5O_4$ (379.37): C, 60.15; H, 4.52; N, 18.46; found: C, 60.19; H, 4.50; N, 18.48.

*3.1.2.4 N′-(3-Hydroxyquinoxalin-2-yl)-1-(4-nitrophenyl)-5-oxopyrrolidine-3-carbohydrazide, **27**.* Light brown powder; yield: (73%), m.p. 267–268 °C; IR (KBr, cm^{-1}) = 3480, 3359, 3219 (br. 2NH & OH), 3078 (CH aromatic), 1698 (br. 2C═O; ^{1}H NMR (400 MHz,$CDCl_3$): δ = 12.86 (s, 1H, OH), 10.79 (d, J = 6.8 Hz, 1H, –NH–**NH**–CO), 8.88 (d, J = 6.6 Hz, 1H, –**NH**–NH–CO), 8.09 (d, J = 7.8 Hz, 2H, A–H), 7.91 (dd, J = 7.7, 1.8 Hz, 1H, A–H), 7.73–7.42 (m, 5H, A–H), 4.20 (dd, J = 12.5, 3.7 Hz, 1H, pyrrolidine **C**H_2), 3.94 (dd, J = 12.5, 3.6 Hz, 1H, pyrrolidine **C**H_2), 3.28–3.16 (m, 1H, pyrrolidine **C**H), 2.71 (dd, J = 15.7, 4.9 Hz, 1H, pyrrolidine **C**H_2), 2.49 (dd, J = 15.6, 4.9 Hz, 1H, pyrrolidine **C**H_2); ^{13}C NMR (100 MHz,$CDCl_3$): δ = 172.73 (C═O), 171.24 (C═O), 146.52, 143.90, 141.54, 139.45, 136.97, 136.51, 128.93, 126.45, 125.38, 124.48, 123.42, 119.11, 48.60 (pyrrolidine **C**H_2), 38.03 (pyrrolidine **C**H), 36.42 (pyrrolidine **C**H_2); MS(EI, 70 eV): m/z (%) = 408.60 [$M^{\bullet+}$] (13.86%), 147.50 (100%); anal. calc. for: $C_{19}H_{16}N_6O_5$ (408.37): C, 55.88; H, 3.95; N, 20.58; found: C, 55.86; H, 3.96; N, 20.55.

Conjugates **28–31** were afforded by reacting 2-chloro-3-hydrazinylquinoxaline (**6**) with fragments **18–21**.

*3.1.2.5 N′-(3-Chloroquinoxalin-2-yl)-1-(4-cyanophenyl)-5-oxopyrrolidine-3-carbohydrazide, **28**.* Brown powder; yield: (66%), m.p. 258–259 °C; IR (KBr, cm^{-1}) = 3367–3260 (br. 2NH), 3070 (CH aromatic), 2213 (CN), 1696 (br. 2C═O); ^{1}H NMR (400 MHz,$CDCl_3$): δ = 10.33 (d, J = 7.0 Hz, 1H, –NH–**NH**–CO), 8.97 (d, J = 7.0 Hz, 1H, **NH**–NH–CO), 8.01–7.86 (m, 2H, A–H), 7.61–7.51 (m, 4H, A–H), 7.30 (d, J = 7.7 Hz, 2H, A–H), 4.19 (dd, J = 12.5, 3.7 Hz, 1H, pyrrolidine CH_2), 3.94 (dd, J = 12.5, 3.6 Hz, 1H, pyrrolidine CH_2), 3.26–3.17 (m, 1H, pyrrolidine CH), 2.71 (dd, J = 15.7, 5.0 Hz, 1H, pyrrolidine CH_2), 2.49 (dd, J = 15.7, 4.9 Hz, 1H, pyrrolidine CH_2); ^{13}C NMR (100 MHz,$CDCl_3$): δ = 172.24 (C═O), 171.54 (C═O), 146.11, 141.32, 140.42, 137.80, 132.33, 131.31, 129.74, 127.06, 126.42, 125.81, 117.89, 117.18 (CN), 102.13, 48.78 (pyrrolidine **C**H_2), 38.09 (pyrrolidine **C**H), 36.37 (pyrrolidine **C**H_2); anal. calc. for: $C_{20}H_{15}ClN_6O_2$ (406.83): C, 59.05; H, 3.72; N, 20.66; found: C, 59.08; H, 3.70; N, 20.65.

*3.1.2.6 N′-(3-Chloroquinoxalin-2-yl)-1-(2,5-dimethylphenyl)-5-oxopyrrolidine-3-carbohydrazide, **29**.* Light brown powder; yield: (75%), m.p. 274–276 °C; IR (KBr, cm^{-1}) = 3349 (br. 2NH), 3044 (CH aromatic), 2904, 2840 (CH aliphatic), 1656 (br. 2C═O; ^{1}H NMR (400 MHz, $CDCl_3$): δ = 10.50 (d, J = 7.0 Hz, 1H, –NH–**NH**–CO), 8.16–8.01 (m, 2H, A–H), 7.94 (d, J = 7.0 Hz, 1H, **NH**–NH–CO), 7.61 (dd, J = 6.0, 3.6 Hz, 2H, A–H), 7.14 (d, J = 8.7 Hz, 1H, A–H), 7.00 (d, J = 7.3 Hz, 2H, A–H), 4.18 (dd, J = 12.2, 3.6 Hz, 1H, pyrrolidine CH_2), 3.93 (dd, J = 12.3, 3.6 Hz, 1H, pyrrolidine CH_2), 3.18–3.09 (m, 1H, pyrrolidine CH), 2.53 (dd, J = 15.6, 4.9 Hz, 1H, pyrrolidine CH_2), 2.34 (dd, J = 15.6, 4.9 Hz, 1H, pyrrolidine CH_2), 2.26 (s, 3H, CH_3), 2.09 (s, 3H, CH_3); ^{13}C NMR (100 MHz,$CDCl_3$): δ = 172.15 (C═O), 171.54 (C═O), 146.11, 140.42, 137.80, 137.35, 132.42, 131.31, 129.74, 129.63, 129.36, 127.06, 126.42, 125.81, 123.84, 121.82, 49.31 (pyrrolidine **C**H_2), 38.12 (pyrrolidine **C**H), 36.32 (pyrrolidine **C**H_2), 19.52 (CH_3), 16.53 (CH_3); MS(EI, 70 eV): m/z (%) = 411.38 [M + 2] (24.70%), 409.44 [$M^{\bullet+}$] (33.19%), 259.30 (100%); anal. calc. for: $C_{21}H_{20}ClN_5O_2$ (409.87): C, 61.54; H, 4.92; N, 17.09; found: C, 61.58; H, 4.90; N, 17.14.

*3.1.2.7 N′-(3-Chloroquinoxalin-2-yl)-1-(3-hydroxyphenyl)-5-oxopyrrolidine-3-carbohydrazide, **30**.* Brown powder; yield: (63%), m.p. 278–279 °C; IR (KBr, cm^{-1}) = 3418–3397 (br. 2NH & 2OH), 3076 (CH aromatic), 1651 (br. 2C═O); ^{1}H NMR (400 MHz,$CDCl_3$): δ = 10.27 (d, J = 7.0 Hz, 1H, –NH–**NH**–CO), 9.38 (d, J = 7.0 Hz, 1H, **NH**–NH–CO), 7.81–7.72 (m, 1H, A–H), 7.71–7.61 (m, 1H, A–H), 7.49–7.39 (m, 3H, A–H & OH), 7.06–6.97 (m, 2H, A–H), 6.55–6.49 (m, 1H, A–H), 6.43–6.34 (m, 1H, A–H), 4.24 (dd, J = 12.5, 3.7 Hz, 1H, pyrrolidine CH_2), 3.98 (dd, J = 12.5, 3.7 Hz, 1H, pyrrolidine CH_2), 3.17–3.09 (m, 1H, pyrrolidine CH), 2.70 (dd, J = 15.6, 4.9 Hz, 1H, pyrrolidine CH_2), 2.45 (dd, J = 15.6, 4.9 Hz, 1H, pyrrolidine CH_2); ^{13}C NMR (100 MHz,$CDCl_3$):δ = 173.48 (C═O), 172.44 (C═O), 158.81, 149.69, 141.26, 140.85, 139.36, 131.53, 131.16, 130.66, 129.32, 126.83, 124.68, 117.35, 109.00, 106.54, 49.02 (pyrrolidine **C**H_2), 40.79 (pyrrolidine **C**H), 38.00 (pyrrolidine **C**H_2); MS(EI, 70 eV):m/z (%) = 397.20 [M + 2] (33.98%), 399.22 [$M^{\bullet+}$] (25.48%), 379.93 (100%); anal. calc. for: $C_{19}H_{16}ClN_5O_3$ (397.82): C, 57.37; H, 4.05; N, 17.60; found: C, 57.33; H, 4.09; N, 17.57.

*3.1.2.8 N′-(3-Chloroquinoxalin-2-yl)-1-(4-nitrophenyl)-5-oxopyrrolidine-3-carbohydrazide, **31**.* Dark yellow powder; yield: (51%), m.p. 266–267 °C; IR (KBr, cm^{-1}) = 3420–3342 (br. 2NH & OH), 3067 (CH aromatic), 1686 (br. 2C═O); ^{1}H NMR (400 MHz,$CDCl_3$): δ = 10.50 (d, J = 7.0 Hz, 1H, –NH–**NH**–CO), 8.15–8.01 (m, 4H, A–H), 7.94 (d, J = 7.0 Hz, 1H, **NH**–NH–CO), 7.61 (dd, J = 6.0, 3.5 Hz, 2H, A–H), 7.40 (d, J = 7.8 Hz, 2H, A–H), 4.17 (dd, J = 12.5, 3.7 Hz, 1H, pyrrolidine CH_2), 3.92 (dd, J = 12.5, 3.6 Hz, 1H, pyrrolidine CH_2), 3.12 (p, J = 4.2 Hz, 1H, pyrrolidine CH), 2.52 (dd, J = 15.7, 4.9 Hz, 1H, pyrrolidine CH_2), 2.33 (dd, J = 15.6, 4.9 Hz, 1H, pyrrolidine CH_2); ^{13}C NMR (100 MHz,$CDCl_3$): δ = 172.65 (C═O), 171.12 (C═O), 146.45, 143.82, 139.83, 139.37, 138.67, 130.84, 129.01, 126.36, 126.02, 125.18, 124.41, 119.04, 48.53 (pyrrolidine **C**H_2), 37.94 (pyrrolidine **C**H), 36.35 (pyrrolidine **C**H_2); MS (EI, 70 eV): m/z (%) = 428.41 [M + 2] (10.83%), 426.69 [$M^{\bullet+}$] (19.33%), 263.76 (100%); anal. calc. for:

$C_{19}H_{15}ClN_6O_4$ (426.82): C, 53.47; H, 3.54; N, 19.69; Found: C, 53.44; H, 3.50; N, 19.67.

3.2. Biology

3.2.1. Agar diffusion approach. The action of the antibacterial was assessed utilizing the well-diffusion of Agar test (Sabaraud Dextrose Agar plates (fungi) and Tryptic Soya Agar plates (bacteria)) (Oxoid Ltd, UK). Eight different hybrids were examined for antimicrobial action taken in opposition to test organisms, namely, Gram-positive bacteria (Methicillin sensitive *S. aureus* (MSSA) ATCC 25923), Bacteria that are Gram-negative (*P. aeruginosa* ATCC 27853, *A. baumannii* ATCC 19606, *K. pneumonia* ATCC 700603, *E. coli* ATCC 25922), and fungal strain (*C. albicans* ATCC 10231). Fresh cultures were utilized to create the bacterial suspensions, which were then adjusted with saline to 0.5 McFarland-standard (pertaining to 1×10^8 CFU mL^{-1}). To attain an ultimate accumulation of 1×10^6 CFU mL^{-1}, the fungal suspensions were likewise modified. A target concentration of 5 mM was obtained by dissolving the investigated hybrids in DMSO. 200 μL of each hybrid were applied. Measurements of surrounding clear zones of inhibition were taken and compared to the negative command. Dimethylsulphoxide (DMSO) functioned as a negative control. Fluconazole as well as Levofloxacin were utilized as standard. Incubation of the plates lasted 24 hours for bacteria and 48 hours for fungus at 35 ± 2 °C. The data were asserted using the well-diffusion technique in triplicate.[84–86]

3.2.2. Evaluation of MIC. 96-well microtiter plates with serial dilutions of the hybrids in Tryptic Soy Broth (TSB-Sigma®) medium were employed to measure the compounds' MIC implementing the broth microdilution method (BMM). The hybrids were prepared as stock solutions in DMSO/TSB 1 : 10 v/v. The concentrations varied between 1.5 and 200 μg mL^{-1}, with fluconazole, levofloxacin, and amoxicillin serving as drug controls. Briefly, in a microtiter plate, 100 μL of the chemicals to be tested were combined with 100 μL of TSB and 5 μL of 1×10^8 CFU mL^{-1} of the strain under investigation. For bacteria or fungi, incubation of the plates lasted at 35 ± 2 °C for 24 or 48 hours, respectively. MIC was the least amount of concentration of substance which showed no signs of growth.[87–90]

3.2.3. Evaluation of MBC and MFC. After transferring 10 μL of MIC-tests culture either plates of Tryptic Soya-Agar or Sabouraud Dextrose-Agar and incubating them overnight at 35 ± 2 °C for 24 hours or 48 hours for bacteria or fungi, MBC and MFC of the substances under test were identified. MBC/MFC is clearly the lowest concentration, resulting in a 99.9% decrease in the growth of bacteria. If the MBC to MIC or MFC to MIC rate falls between 1 : 1 and 2 : 1, the investigated conjugate was deemed bactericidal or fungicidal; if the ratio is more than 2 : 1, it was deemed bacteriostatic or fungistatic.[91–95]

3.2.4. Anti-biofilm activity. Using TSB, the inhibitory impact of studied hybrids on biofilm development was evaluated in 96-well polystyrene flat-bottom plates. Briefly, 200 μL of freshly inoculated TSB with 1% glucose was aliquoted into plate wells, resulting in a last focus of 10^6 CFU per mL of the tested strain. The culture was conducted in the presence of sub-inhibitory doses (50 and 90% of MIC). To remove all of the planktonic bacterial cells, the cups had next cultured for 24 hours at 37 °C, after that washed three times with PBS. Following the washing stage, the cups had opened inside a hot air at 60 °C for 60 minutes, then 150 μL of crystal-violet (CV) at a 0.1% concentration was put into every well for 15 minutes for fixing and staining. To get rid of any remaining CV stains, the washing process was reapplied Addition of 150 μL of 100% ethanol to each well followed the washing process and the well OD at 630 nm was measured in a 96-well plate spectrophotometer (800 TS Absorbance Reader, Biotek, USA). Every plate included sterility and growth controls. Ultimately, The formula below was utilized to ascertain the inhibitory percentages of biofilm: biofilm inhibitory (%) = [1 − OD nm isolate/OD nm of positive control] × 100.[96–103]

3.2.5. Time kill kinetics. The bactericidal efficacy of the conjugates under evaluation was confirmed by the time-kill experiment. *P. auerogenosa* ATCC 27853 bacterial cultures in the exponential growth phase (1×10^6 CFU mL^{-1}) were administered treatment in drug-containing tubes under examination at 8-fold, 4-fold, 2-fold, 1-fold and 0.5-fold MIC, and incubated at 37 °C. Viable count measurements were made using samples collected at 0, 3, 6, 12, and 24 hours of incubation. After being serially diluted, each sample was spread out across two to four agar plates. CFU were established following 18 to 24 hours of the incubated at 35 °C in 5% CO_2. 10 CFU mL^{-1} was the limit of detection (LOD). Visual examination of the colony dispersion on the plates was used to gauge drug carryover. Growth control was included, involving an experiment without addition of hybrids. A plot of log 10 CFU mL^{-1} *vs.* time (h) was used to depict the bactericidal kinetics of conjugates.[104–109]

3.2.6. DNA gyrase inhibition assay. See SI.[110–115]

3.3. *In silico* ADMET

Pharmacokinetics prediction was performed as reported.[116–123]

3.4. Molecular docking

The 3D layout for DNA gyrase (PDB.: 8BN6) had been extracted through data bank of the protein (https://www.rcsb.org/) and prepared using UCSF Chimera.[124–127] Briefly, the mol2 file of protein was set by deleting water molecules, adding and charges and energy minimization. The generated compounds and respective co-crystallized ligands were sketched in Avogadro software, and their geometries were optimized.[128,129] The prepared protein was imported in AutoDock. Hydrogens were added and Kollman charges and AD4 atom parameters were assigned. The grid calculations were set up; −5.5 × 23.5 × 1.1 Å grid with dimensions of 35, 35, 35 respectively, at a resolution of 0.375 Å, was created around the compound. Docking commenced using genetic algorithm search parameters. During docking, partial Gasteiger charges were applied. Docked conformations were generated using the Lamarckian evolutionary method and arranged according to their docking energy in descending order.[130–134] Results visualizations were performed using Biovia Discovery Studio. The same steps were

repeated for the co-crystallized ligand in order to perform validation. The RMSD value of the redocked pose was calculated using DockRMSD online tool.[135,136]

4. Conclusion

This study successfully synthesized and studied several novel hybrid chemicals, such as quinoxaline, pyrrolidine, and a hydrazinyl bridge, indicating their potential as strong antibacterial and antifungal medicines. Several compounds had strong efficacy against different pathogenic strains, according to the *in vitro* tests, with eight derivatives demonstrating notable bactericidal effects. Eight novel conjugates were tested for antibacterial activity at a dosage of 5 mM. All synthesized derivatives caused *E. coli* growth ZOI ≥15 mm, with hybrids **26**, **28**, **30**, and **31** showing greater reduction than Amoxicillin and Levofloxacin. Hybrids **24**, **27**, and **29** were confirmed as bactericidal agents against *E. coli*. Hybrids **24**, **25**, and **31** displayed MIC of 12.5 μM, whereas they indicate bactericidal hybrids at higher concentrations against *P. aeruginosa*. Treatment with involving all hybrids resulted in 89–92% decrease in biofilm formation at 90% MIC, outperforming Levofloxacin. The killing kinetics of eight hybrids against *P. aeruginosa* were time-dependent, with higher concentrations leading to a rapid decrease in CFU number. Primary bacterial elimination occurred after 3 hours, while 4-fold and 8-fold MICs led to almost complete elimination. Hybrids **25**, **28**, and **31** were the most efficient DNA gyrase inhibitors; their IC50 values were significantly lower than those of ciprofloxacin (77.3, 87.6, and 65.5 μM). The study reveals that molecular docking studies reveal effective compounds' binding interactions, confirming their biological activities. Compounds having drug-like properties are identified by examining their physicochemical and pharmacokinetic properties, indicating the possibility of further development. With future research concentrating on optimizing lead compounds for clinical applications, the findings support the continuing attempts to develop novel treatment medicines for infectious disorders and resistant microbial strains.

Conflicts of interest

The author(s) report no conflicts of interest in this work.

Data availability

The data supporting this article have been included as part of the supplementary information (SI). Supplementary information is available. See DOI: https://doi.org/10.1039/d6ra00675b.

References

1 T. M. Rawson, R. C. Wilson and A. Holmes, Understanding the role of bacterial and fungal infection in COVID-19, *Clin. Microbiol. Infection*, 2021, **27**, 9–11.
2 J. R. Köhler, B. Hube, R. Puccia, A. Casadevall and J. R. Perfect, Fungi that Infect Humans, *Microbiol. Spectr.*, 2017, **5**(3), DOI: 10.1128/microbiolspec.FUNK-0014-2016.
3 J. Verhoef, K. van Kessel and H. Snippe, Immune Response in Human Pathology: Infections Caused by Bacteria, Viruses, Fungi, and Parasites, in *Nijkamp and Parnham's Principles of Immunopharmacology*, ed. M. J. Parnham, F. P. Nijkamp and A. G. Rossi, Springer International Publishing, Cham, 2019, pp. 165–178.
4 B. M. Peters, M. A. Jabra-Rizk, G. A. O'May, J. W. Costerton and M. E. Shirtliff, Polymicrobial Interactions: Impact on Pathogenesis and Human Disease, *Clin. Microbiol. Rev.*, 2012, **25**, 193–213.
5 G. Muteeb, M. T. Rehman, M. Shahwan and M. Aatif, Origin of Antibiotics and Antibiotic Resistance, and Their Impacts on Drug Development: A Narrative Review, *Pharmaceuticals*, 2023, **16**, 1615.
6 M. Terreni, M. Taccani and M. Pregnolato, New Antibiotics for Multidrug-Resistant Bacterial Strains: Latest Research Developments and Future Perspectives, *Molecules*, 2021, **26**, 2671.
7 R. L. Monaghan and J. F. Barrett, Antibacterial drug discovery—Then, now and the genomics future, *Biochem. Pharmacol.*, 2006, **71**, 901–909.
8 J. Murugaiyan, P. A. Kumar, G. S. Rao, K. Iskandar, S. Hawser, J. P. Hays, *et al.*, Progress in Alternative Strategies to Combat Antimicrobial Resistance: Focus on Antibiotics, *Antibiotics*, 2022, **11**, 200.
9 M. Frieri, K. Kumar and A. Boutin, Antibiotic resistance, *J. Infect. Public Health*, 2017, **10**, 369–378.
10 A. Tarín-Pelló, B. Suay-García and M.-T. Pérez-Gracia, Antibiotic resistant bacteria: current situation and treatment options to accelerate the development of a new antimicrobial arsenal, *Expert Rev. Anti-infect. Ther.*, 2022, **20**, 1095–1108.
11 D. Chinemerem Nwobodo, M. C. Ugwu, C. Oliseloke Anie, M. T. S. Al-Ouqaili, J. Chinedu Ikem, U. Victor Chigozie, *et al.*, Antibiotic resistance: The challenges and some emerging strategies for tackling a global menace, *J. Clin. Lab. Anal.*, 2022, **36**, e24655.
12 M. A. Salam, M. Y. Al-Amin, M. T. Salam, J. S. Pawar, N. Akhter, A. A. Rabaan, *et al.*, Antimicrobial Resistance: A Growing Serious Threat for Global Public Health, *Healthcare*, 2023, **11**, 1946.
13 T. Ramsis, H. M. Refat, M. Selim, H. Elseedy and E. A. Fayed, The role of current synthetic and possible plant and marine phytochemical compounds in the treatment of acne, *RSC Adv.*, 2024, **14**, 24287–24321.
14 E. A. Fayed, S. A. El-Sebaey, M. A. Ebrahim, K. Abu-Elfotuh, R. El-Sayed Mansour, E. K. Mohamed, *et al.*, Discovery of novel bicyclic and tricyclic cyclohepta[b]thiophene derivatives as multipotent AChE and BChE inhibitors, in-Vivo and in-Vitro assays, ADMET and molecular docking simulation, *Eur. J. Med. Chem.*, 2025, **284**, 117201.
15 M. S. Abusaif, A. Ragab, E. A. Fayed, Y. A. Ammar, A. M. H. Gowifel, S. O. Hassanin, *et al.*, Exploring a novel thiazole derivatives hybrid with fluorinated-

indenoquinoxaline as dual inhibitors targeting VEGFR2/AKT and apoptosis inducers against hepatocellular carcinoma with docking simulation, *Bioorg. Chem.*, 2025, **154**, 108023.

16 R. Hassan, R. Mohi-ud-din, M. O. Dar, A. J. Shah, P. A. Mir, M. Shaikh, *et al.*, Bioactive Heterocyclic Compounds as Potential Therapeutics in the Treatment of Gliomas: A Review, *Anti-Cancer Agents Med. Chem.*, 2022, **22**, 551–565.

17 E. A. Fayed, A. Thabet, S. M. A. El-Gilil, H. M. A. Elsanhory and Y. A. Ammar, Fluorinated thiazole–thiosemicarbazones hybrids as potential PPAR-γ agonist and α-amylase, α-glucosidase antagonists: Design, synthesis, in silico ADMET and docking studies and hypoglycemic evaluation, *J. Mol. Struct.*, 2024, **1301**, 137374.

18 S. E. Desouky, M. Abu-Elghait, E. A. Fayed, S. Selim, B. Yousuf, Y. Igarashi, *et al.*, Secondary Metabolites of Actinomycetales as Potent Quorum Sensing Inhibitors Targeting Gram-Positive Pathogens: In Vitro and In Silico Study, *Metabolites*, 2022, **12**, 246.

19 B. A. AbdelFattah, M. M. A. Khalifa, H. El-Sehrawi, E. Fayed, A. Bayoumi and M. Said, Synthesis and Anxiolytic Activity of Some Novel 5-oxo-1, 4-oxazepine Derivatives, *Lett. Drug Des. Discovery*, 2011, **8**, 330–338.

20 H. Li, Y.-H. He, Y.-M. Hu, Q.-R. Chu, Y.-J. Chen, Z.-R. Wu, *et al.*, Design, Synthesis, and Structure–Activity Relationship Studies of Magnolol Derivatives as Antifungal Agents, *J. Agric. Food Chem.*, 2021, **69**, 11781–11793.

21 N. J. C. Oliveira, I. N. S. Teixeira, P. O. Fernandes, G. C. Veríssimo, A. D. Valério, C. P. D. S. Moreira, *et al.*, Computer-aided molecular design, synthesis and evaluation of antifungal activity of heterocyclic compounds, *J. Mol. Struct.*, 2022, **1267**, 133573.

22 B. A. Abdel Fattah, M. M. A. Khalifa, H. El-Sehrawi and E. Fayed, Synthesis, Anxiolytic and Antimicrobial Activity of Some Novel 5-oxo-1, 4-Oxazepine Derivatives, *Egypt. J. Biomed. Sci.*, 2010, **33**, 269.

23 Y. U. Cebeci, Ö. Ö. Batur and H. Boulebd, Design, synthesis, theoretical studies, and biological activity evaluation of new nitrogen-containing poly heterocyclic compounds as promising antimicrobial agents, *J. Mol. Struct.*, 2024, **1299**, 137115.

24 U. Fathy, H. A. Abd El Salam, E. A. Fayed, A. M. Elgamal and A. Gouda, Erratum to "Facile synthesis and in vitro anticancer evaluation of a new series of tetrahydroquinoline" [Heliyon 7(10) (October 2021) e08117] (Heliyon (2021) 7(10), (S2405844021022209), *Heliyon*, 2024, **10**(1), e23189, DOI: 10.1016/j.heliyon.2021.e08117.

25 T. Z. Shawer and E. A. Fayed, Synthesis, docking and anticancer activity of some new thienopyrimidine and thienooxazine derivatives, *Nat. Sci.*, 2014, **12**(12), 171–181.

26 M. Montana, V. Montero, O. Khoumeri and P. Vanelle, Quinoxaline derivatives as antiviral agents: a systematic review, *Molecules*, 2020, **25**, 2784.

27 T. M. Ramsis, S. E. Abdel Karim, N. Vassilaki, E. Frakolaki, A. A. M. Kamal, G. Zoidis, *et al.*, Expanding the chemical space of anti-HCV NS5A inhibitors by stereochemical exchange and peptidomimetic approaches, *Arch. Pharmazie*, 2018, **351**, 1800017.

28 N. A. Gohar, E. A. Fayed, Y. A. Ammar, O. A. Abu Ali, A. Ragab, A. M. Mahfoz, *et al.*, Fluorinated indenoquinoxaline bearing thiazole moieties as hypoglycaemic agents targeting α-amylase, and α-glucosidase: synthesis, molecular docking, and ADMET studies, *J. Enzyme Inhib. Med. Chem.*, 2024, **39**, 2367128.

29 A. Thabet, M. Samir Abusaif, Y. A. Ammar, S. M. Abd-Elgilil and H. Elsanhory, Bis-thiazole hybrids as promising candidates in controlling diabetes mellitus in vivo, in vitro evaluation, in silico ADMET, and docking studies, *Al-Azhar Int. J. Pharm. Med. Sci.*, 2025, **5**(2), 87–105.

30 S. Tariq, K. Somakala and M. Amir, Quinoxaline: An insight into the recent pharmacological advances, *Eur. J. Med. Chem.*, 2018, **143**, 542–557.

31 E. A. Fayed, N. A. Gohar, A. M. Farrag and Y. A. Ammar, Upregulation of BAX and caspase-3, as well as downregulation of Bcl-2 during treatment with indeno [1,2-b]quinoxalin derivatives, mediated apoptosis in human cancer cells, *Arch. Pharmazie*, 2022, **355**, 2100454.

32 A. Mishra, V. Jha and H. Rajak, Molecular structural investigations of quinoxaline derivatives through 3D-QSAR, molecular docking, ADME prediction and pharmacophore modeling studies for the search of novel antimalarial agent, *J. Indian Chem. Soc.*, 2022, **99**, 100343.

33 Y. Singh, N. Kumar, S. Kulkarni, S. Singh and S. Thareja, Pharmacophore derived 3D-QSAR, molecular docking, and simulation studies of quinoxaline derivatives as ALR2 inhibitors, *J. Biomol. Struct. Dyn.*, 2024, **42**, 10452–10488.

34 S. K. Suthar, N. S. Chundawat, G. P. Singh, J. M. Padrón and Y. K. Jhala, Quinoxaline: A comprehension of current pharmacological advancement in medicinal chemistry, *Eur. J. Med. Chem. Rep.*, 2022, **5**, 100040.

35 S. ElKalyoubi and E. Fayed, Synthesis and Evaluation of Antitumour Activities of Novel Fused Tri- and Tetracyclic Uracil Derivatives, *J. Chem. Res.*, 2016, **40**, 771–777.

36 U. Fathy, H. A. Abd El Salam, E. A. Fayed, A. M. Elgamal and A. Gouda, Facile synthesis and anticancer evaluation of a new series of tetrahydroquinoline, *Heliyon*, 2021, **7**, e08117.

37 E. Fayed and H. Ahmed, Synthesis, characterization and pharmacological evaluation of some new 1, 4-diazepine derivatives as anticancer agents, *Pharma Chem.*, 2016, **8**, 77–90.

38 A. Sharma, A. Deep, M. G. Marwaha and R. K. Marwaha, Quinoxaline: A chemical moiety with spectrum of interesting biological activities, *Mini Rev. Med. Chem.*, 2022, **22**, 927–948.

39 K. Otoguro, A. Ishiyama, M. Iwatsuki, M. Namatame, A. Nishihara-Tukashima, T. Nakashima, *et al.*, In vitro and in vivo anti-Trypanosoma brucei activities of phenazinomycin and related compounds, *J. Antibiotics*, 2010, **63**, 579–581.

40 F. Xu and J. A. McCauley, Discovery and Chemical Development of Grazoprevir: An HCV NS3/4a Protease

Inhibitor for the Treatment of the Hepatitis C Virus Infection, in *Complete Accounts of Integrated Drug Discovery and Development: Recent Examples from the Pharmaceutical Industry Volume 3*, American Chemical Society, 2020, vol. 1369, pp. 285–312.

41 S. Wang, Y. Wang, J. Wang, T. Sato, K. Izawa, V. A. Soloshonok, *et al.*, The Second-generation of Highly Potent Hepatitis C Virus (HCV) NS3/4A Protease Inhibitors: Evolutionary Design Based on Tailor-made Amino Acids, Synthesis and Major Features of Bio-activity, *Curr. Pharm. Des.*, 2017, **23**, 4493–4554.

42 J. G. Taylor, S. Zipfel, K. Ramey, R. Vivian, A. Schrier, K. K. Karki, *et al.*, Discovery of the pan-genotypic hepatitis C virus NS3/4A protease inhibitor voxilaprevir (GS-9857): A component of Vosevi®, *Bioorg. Med. Chem. Lett.*, 2019, **29**, 2428–2436.

43 D. Nageswara Rao, J. Zephyr, M. Henes, E. T. Chan, A. N. Matthew, A. K. Hedger, *et al.*, Discovery of Quinoxaline-Based P1–P3 Macrocyclic NS3/4A Protease Inhibitors with Potent Activity against Drug-Resistant Hepatitis C Virus Variants, *J. Med. Chem.*, 2021, **64**, 11972–11989.

44 L. Yurttaş, Y. Özkay, Z. A. Kaplancıklı, Y. Tunalı and H. Karaca, Synthesis and antimicrobial activity of some new hydrazone-bridged thiazole-pyrrole derivatives, *J. Enzyme Inhib. Med. Chem.*, 2013, **28**, 830–835.

45 R. H. Abd El-Hameed, A. I. Sayed, S. Mahmoud Ali, M. A. Mosa, Z. M. Khoder and S. S. Fatahala, Synthesis of novel pyrroles and fused pyrroles as antifungal and antibacterial agents, *J. Enzyme Inhib. Med. Chem.*, 2021, **36**, 2183–2198.

46 P. Rawat, R. Singh, A. Ranjan, A. Gautam, S. Trivedi and M. Kumar, Study of antimicrobial and antioxidant activities of pyrrole-chalcones, *J. Mol. Struct.*, 2021, **1228**, 129483.

47 E. A. Fayed, N. A. Gohar, A. H. Bayoumi and Y. A. Ammar, Novel fluorinated pyrazole-based heterocycles scaffold: cytotoxicity, in silico studies and molecular modelling targeting double mutant EGFR L858R/T790M as antiproliferative and apoptotic agents, *Med. Chem. Res.*, 2023, **32**, 369–388.

48 C. Y. Hong, Discovery of gemifloxacin (Factive, LB20304a): a quinolone of new a generation, *Il Farmaco*, 2001, **56**, 41–44.

49 J.-P. Caeiro and P. B. Iannini, Moxifloxacin (Avelox®): a novel fluoroquinolone with a broad spectrum of activity, *Expert Rev. Anti-infect. Ther.*, 2003, **1**, 363–370.

50 U. Fathy, M. N. M. Yousif, E. M. Mohi El-Deen and E. Fayed, Design, Synthesis, and biological evaluation of a novel series of thiazole derivatives based on pyrazoline as anticancer agents, *Egypt. J. Chem.*, 2022, **65**, 1241–1252.

51 S. Kiyotoki, J. Nishikawa and I. Sakaida, Efficacy of vonoprazan for Helicobacter pylori eradication, *Intern. Med.*, 2020, **59**, 153–161.

52 A. Rusu, I.-M. Moga, L. Uncu and G. Hancu, The Role of Five-Membered Heterocycles in the Molecular Structure of Antibacterial Drugs Used in Therapy, *Pharmaceutics*, 2023, **15**, 2554.

53 T. M. Ramsis, S. Hussein, M. S. Abusaif, A. Ragab, Y. A. Ammar, O. Ali, *et al.*, Bridging the gap with amide linkers: rational design, synthesis, and multi-target evaluation of sulfonamide/acetamide-NSAID hybrids as dual COX-2/5-LOX inhibitors, *Future Med. Chem.*, 2026, **18**, 131–148.

54 M. N. Matada, K. Jathi, M. M. Rangappa, K. Geoffry, S. R. Kumar, R. B. Nagarajappa, *et al.*, A new sulphur containing heterocycles having azo linkage: Synthesis, structural characterization and biological evaluation, *J. King Saud Univ. Sci.*, 2020, **32**, 3313–3320.

55 T. Tahir, M. Ashfaq, M. Saleem, M. Rafiq, M. I. Shahzad, K. Kotwica-Mojzych, *et al.*, Pyridine scaffolds, phenols and derivatives of azo moiety: current therapeutic perspectives, *Molecules*, 2021, **26**, 4872.

56 K. Mezgebe and E. Mulugeta, Synthesis and pharmacological activities of azo dye derivatives incorporating heterocyclic scaffolds: a review, *RSC Adv.*, 2022, **12**, 25932–25946.

57 S. A. El-Kalyoubi, E. A. Fayed and A. S. Abdel-Razek, One pot synthesis, antimicrobial and antioxidant activities of fused uracils: pyrimidodiazepines, lumazines, triazolouracil and xanthines, *Chem. Cent. J.*, 2017, **11**, 66.

58 T. Khan, K. Sankhe, V. Suvarna, A. Sherje, K. Patel and B. Dravyakar, DNA gyrase inhibitors: Progress and synthesis of potent compounds as antibacterial agents, *Biomed. Pharmacother.*, 2018, **103**, 923–938.

59 A. Duprey and E. A. Groisman, DNA supercoiling differences in bacteria result from disparate DNA gyrase activation by polyamines, *PLoS Genet.*, 2020, **16**, e1009085.

60 G. Sanyal and P. Doig, Bacterial DNA replication enzymes as targets for antibacterial drug discovery, *Expet Opin. Drug Discov.*, 2012, **7**, 327–339.

61 G. Seneviratne, J. S. Zavahir, W. Bandara and M. Weerasekara, Fungal-bacterial biofilms: their development for novel biotechnological applications, *World J. Microbiol. Biotechnol.*, 2008, **24**, 739–743.

62 D. C. Sheppard and P. L. Howell, Biofilm Exopolysaccharides of Pathogenic Fungi: Lessons from Bacteria, *J. Biol. Chem.*, 2016, **291**, 12529–12537.

63 F. M. Carvalho, A. Azevedo, M. M. Ferreira, F. J. M. Mergulhão and L. C. Gomes, Advances on Bacterial and Fungal Biofilms for the Production of Added-Value Compounds, *Biology*, 2022, **11**, 1126.

64 H. Van Acker, P. Van Dijck and T. Coenye, Molecular mechanisms of antimicrobial tolerance and resistance in bacterial and fungal biofilms, *Trends Microbiol.*, 2014, **22**, 326–333.

65 E. A. Fayed, M. A. Ebrahim, U. Fathy, H. S. El Saeed and W. S. Khalaf, Evaluation of quinoxaline derivatives as potential ergosterol biosynthesis inhibitors: design, synthesis, ADMET, molecular docking studies, and antifungal activities, *J. Mol. Struct.*, 2022, **1267**, 133578.

66 R. M. Donlan and J. W. Costerton, Biofilms: survival mechanisms of clinically relevant microorganisms, *Clin. Microbiol. Rev.*, 2002, **15**, 167–193.
67 S. T. Asma, K. Imre, A. Morar, V. Herman, U. Acaroz, H. Mukhtar, *et al.*, An overview of biofilm formation–combating strategies and mechanisms of action of antibiofilm agents, *Life*, 2022, **12**, 1110.
68 A. R. Bhat, R. S. Dongre, A. H. Shalla, G. A. Naikoo and I. U. Hassan, Computational analysis for antimicrobial active pyrano [2, 3-d] pyrimidine derivatives on the basis of theoretical and experimental ground, *J. Assoc. Arab Univ. Basic Appl. Sci.*, 2016, **20**, 19–25.
69 M. A. Ebrahim, T. M. Ramsis, N. A. Gohar, S. A. metwally, A. Rushdi and E. A. Fayed, Novel Pyrrolidine-bearing quinoxaline inhibitors of DNA Gyrase, RNA polymerase and spike glycoprotein, *Bioorg. Chem.*, 2025, **156**, 108218.
70 K. H. Oudah, M. A. A. Najm, T. M. Ramsis, M. A. Ebrahim, N. A. Gohar, K. Abu-Elfotuh, *et al.*, Unlocking Therapeutic Potential of Novel Thieno-Oxazepine Hybrids as Multi-Target Inhibitors of AChE/BChE and Evaluation Against Alzheimer's Disease: In Vivo, In Vitro, Histopathological, and Docking Studies, *Pharmaceuticals*, 2025, **18**, 1214.
71 A. S. Oyedele, D. N. Bogan and C. O. Okoro, Synthesis, biological evaluation and virtual screening of some acridone derivatives as potential anticancer agents, *Bioorg. Med. Chem.*, 2020, **28**, 115426.
72 M. Y. Refai, A. M. Elazzazy, S. E. Desouky, M. Abu-Elghait, E. A. Fayed, S. M. Alajel, *et al.*, Interception of Epoxide ring to quorum sensing system in Enterococcus faecalis and Staphylococcus aureus, *AMB Express*, 2023, **13**, 126.
73 D. E. V. Pires, T. L. Blundell and D. B. Ascher, pkCSM: Predicting Small-Molecule Pharmacokinetic and Toxicity Properties Using Graph-Based Signatures, *J. Med. Chem.*, 2015, **58**, 4066–4072.
74 P. Banerjee, A. O. Eckert, A. K. Schrey and R. Preissner, ProTox-II: a webserver for the prediction of toxicity of chemicals, *Nucleic Acids Res.*, 2018, **46**, W257–W263.
75 S. A. Serkov, N. N. Kostikova, N. V. Sigay, A. P. Tyurin, N. G. Kolotyrkina and G. A. Gazieva, The synthesis and study of antimicrobial activity of 5-oxo-1-(thiazol-2-yl) pyrrolidine-3-carboxylic acids, *Chem. Heterocycl. Compd.*, 2024, **60**, 365–370.
76 P. L. Paytash, M. J. Thompson and M. E. Fykes, Itaconic Acid Derivatives of Sulfanilamide, *J. Am. Chem. Soc.*, 1952, **74**, 4549–4552.
77 K. Inoguchi, T. Morimoto and K. Achiwa, Asymmetric reactions catalyzed by chiral metal complexes: XXXII. Efficient asymmetric hydrogenation of itaconic acid derivatives catalyzed by rhodium complexes of improved (2S,4S)-N-(t-butoxycarbonyl)-4-(diphenylphosphino)-2-[(diphenylphosphino)methyl]pyrrolidine (BPPM) analogues, *J. Organomet. Chem.*, 1989, **370**, C9–C12.
78 G. J. Noordzij and C. H. Wilsens, Cascade aza-Michael addition-cyclizations; toward renewable and multifunctional carboxylic acids for melt-polycondensation, *Front. Chem.*, 2019, **7**, 729.
79 I. Shabeeb, L. Al-Essa, M. Shtaiwi, E. Al-Shalabi, E. Younes, R. Okasha, *et al.*, New Hydrazide-hydrazone Derivatives of Quinoline 3-Carboxylic Acid Hydrazide: Synthesis, Theoretical Modeling and Antibacterial Evaluation, *Lett. Org. Chem.*, 2019, **16**, 430–436.
80 Ł. Popiołek, B. Rysz, A. Biernasiuk and M. Wujec, Synthesis of promising antimicrobial agents: hydrazide-hydrazones of 5-nitrofuran-2-carboxylic acid, *Chem. Biol. Drug Des.*, 2020, **95**, 260–269.
81 K. Paruch, Ł. Popiołek, A. Biernasiuk, A. Berecka-Rycerz, A. Malm, A. Gumieniczek, *et al.*, Novel Derivatives of 4-Methyl-1,2,3-Thiadiazole-5-Carboxylic Acid Hydrazide: Synthesis, Lipophilicity, and In Vitro Antimicrobial Activity Screening, *Appl. Sci.*, 2021, **11**, 1180.
82 M. Y. Kornev, V. S. Moshkin, O. S. Eltsov and V. Y. Sosnovskikh, Reactions of chromone-3-carboxylic acid and chromone-3-carboxamides with cyanoacetic acid hydrazide, *Mendeleev Commun.*, 2016, **26**, 72–74.
83 E. M. Sarshira, N. M. Hamada, Y. M. Moghazi and M. M. Abdelrahman, Synthesis and Biological Evaluation of Some Heterocyclic Compounds from Salicylic Acid Hydrazide, *J. Heterocycl. Chem.*, 2016, **53**, 1970–1982.
84 Clinical and L. S. Institute, *Performance Standards for Antimicrobial Susceptibility Testing*, Clinical and Laboratory Standards Institute, Wayne, PA, 2020.
85 S. A. El-Kalyoubi, E. A. Fayed and A. S. Abdel-Razek, Erratum: One pot synthesis, antimicrobial and antioxidant activities of fused uracils: Pyrimidodiazepines, lumazines, triazolouracil and xanthines," [Chem Cent J 11, (2017) (66)], *Chem. Cent. J.*, 2017, **11**(1), 69, DOI: 10.1186/s13065-017-0294-0.
86 Y. Ammar, E. Fayed, A. Bayoumi and M. Saleh, Synthesis and biological evaluation of new amides pro-drugs containing naproxen moiety as anti-inflammatory and antimicrobial agents, *Pharma Chem.*, 2016, **8**, 495–508.
87 A. J. Cartagena, K. L. Taylor, J. T. Smith, A. L. Manson, V. M. Pierce and A. M. Earl, The carbapenem inoculum effect provides insight into the molecular mechanisms underlying carbapenem resistance in Enterobacterales, *bioRxiv*, 2023, preprint, DOI: 10.1101/2023.05.23.541813.
88 N. Sasoni, B. Caracciolo, M. S. Cabeza, S. Gamarra, S. Carnovale and G. Garcia-Effron, Antifungal susceptibility testing following the CLSI M27 document, along with the measurement of MFC/MIC ratio, could be the optimal approach to detect amphotericin B resistance in *Clavispora (Candida) lusitaniae*. Susceptibility patterns of contemporary isolates of this species, *Antimicrob. Agents Chemother.*, 2024, **68**, e00968–23.
89 C. S. Makade, P. R. Shenoi, B. A. Bhongade, S. A. Shingane, P. C. Ambulkar and A. M. Shewale, Estimation of MBC: MIC Ratio of Herbal Extracts against Common Endodontic Pathogens, *J. Pharm. BioAllied Sci.*, 2024, **16**, S1414–S1416.
90 R. D. de Castro, T. M. P. A. de Souza, L. M. D. Bezerra, G. L. S. Ferreira, E. M. M. de Brito Costa and A. L. Cavalcanti, Antifungal activity and mode of action of thymol and its synergism with nystatin against Candida

species involved with infections in the oral cavity: an in vitro study, *BMC Compl. Alternative Med.*, 2015, **15**, 417.
91 G. Morace, M. Drago, M. M. Scaltrito, S. Conti, F. Fanti and L. Polonelli, In Vitro Activity (MIC and MFC) of Voriconazole, Amphotericin B, and Itraconazole Against 192 Filamentous Fungi: The GISIA-2 Study, *J. Chemother.*, 2007, **19**, 508–513.
92 G. Anand, M. Ravinanthan, R. Basaviah and A. V. Shetty, In vitro antimicrobial and cytotoxic effects of Anacardium occidentale and Mangifera indica in oral care, *J. Pharm. BioAllied Sci.*, 2015, **7**, 69–74.
93 P. Arulmozhi, S. Vijayakumar and T. Kumar, Phytochemical analysis and antimicrobial activity of some medicinal plants against selected pathogenic microorganisms, *Microb. Pathog.*, 2018, **123**, 219–226.
94 S. Rehman, S. M. Asiri, F. A. Khan, B. R. Jermy, H. Khan, S. Akhtar, *et al.*, Biocompatible Tin Oxide Nanoparticles: Synthesis, Antibacterial, Anticandidal and Cytotoxic Activities, *ChemistrySelect*, 2019, **4**, 4013–4017.
95 M. Jalal, M. A. Ansari, M. A. Alzohairy, S. G. Ali, H. M. Khan, A. Almatroudi, *et al.*, Biosynthesis of Silver Nanoparticles from Oropharyngeal Candida glabrata Isolates and Their Antimicrobial Activity against Clinical Strains of Bacteria and Fungi, *Nanomaterials*, 2018, **8**, 586.
96 H. Liu, Y. Zhao, D. Zhao, T. Gong, Y. Wu, H. Han, *et al.*, Antibacterial and anti-biofilm activities of thiazolidione derivatives against clinical staphylococcus strains, *Emerg. Microb. Infect.*, 2015, **4**, 1–6.
97 G. Spengler, A. Kincses, T. Mosolygó, M. A. Marć, M. Nové, M. Gajdács, *et al.*, Antiviral, Antimicrobial and Antibiofilm Activity of Selenoesters and Selenoanhydrides, *Molecules*, 2019, **24**, 4264.
98 Y. Liu, L. Wu, J. Han, P. Dong, X. Luo, Y. Zhang, *et al.*, Inhibition of Biofilm Formation and Related Gene Expression of Listeria monocytogenes in Response to Four Natural Antimicrobial Compounds and Sodium Hypochlorite, *Front. Microbiol.*, 2020, **11**, 617473.
99 N. Tripathi and M. K. Goshisht, Recent Advances and Mechanistic Insights into Antibacterial Activity, Antibiofilm Activity, and Cytotoxicity of Silver Nanoparticles, *ACS Appl. Bio Mater.*, 2022, **5**, 1391–1463.
100 E. Sánchez, C. Rivas Morales, S. Castillo, C. Leos-Rivas, L. García-Becerra and D. M. Ortiz Martínez, Antibacterial and Antibiofilm Activity of Methanolic Plant Extracts against Nosocomial Microorganisms, *Evid. Based Complement. Alternat. Med.*, 2016, **2016**, 1572697.
101 M. M. Bazargani and J. Rohloff, Antibiofilm activity of essential oils and plant extracts against Staphylococcus aureus and Escherichia coli biofilms, *Food Control*, 2016, **61**, 156–164.
102 A. Majumder, C. Sarkar, I. Das, S. Sk, S. Bandyopadhyay, S. Mandal, *et al.*, Design, Synthesis and Evaluation of a Series of Zinc(II) Complexes of Anthracene-Affixed Multifunctional Organic Assembly as Potential Antibacterial and Antibiofilm Agents against Methicillin-Resistant Staphylococcus aureus, *ACS Appl. Mater. Interfaces*, 2023, **15**, 22781–22804.
103 R. Gondru, K. Sirisha, S. Raj, S. K. Gunda, C. G. Kumar, M. Pasupuleti, *et al.*, Design, Synthesis, In Vitro Evaluation and Docking Studies of Pyrazole-Thiazole Hybrids as Antimicrobial and Antibiofilm Agents, *ChemistrySelect*, 2018, **3**, 8270–8276.
104 Z. Zhang, K. Li, G.-Y. Zhang, Y.-Z. Tang and Z. Jin, Design, synthesis and biological activities of novel pleuromutilin derivatives with a substituted triazole moiety as potent antibacterial agents, *Eur. J. Med. Chem.*, 2020, **204**, 112604.
105 A. M. Shehabeldine, B. H. Amin, F. A. Hagras, A. A. Ramadan, M. R. Kamel, M. A. Ahmed, *et al.*, Potential Antimicrobial and Antibiofilm Properties of Copper Oxide Nanoparticles: Time-Kill Kinetic Essay and Ultrastructure of Pathogenic Bacterial Cells, *Appl. Biochem. Biotechnol.*, 2023, **195**, 467–485.
106 T. Appiah, Y. D. Boakye and C. Agyare, Antimicrobial Activities and Time-Kill Kinetics of Extracts of Selected Ghanaian Mushrooms, *Evid. Based Complement. Alternat. Med.*, 2017, **2017**, 4534350.
107 S. Foerster, M. Unemo, L. J. Hathaway, N. Low and C. L. Althaus, Time-kill curve analysis and pharmacodynamic modelling for in vitro evaluation of antimicrobials against Neisseria gonorrhoeae, *BMC Microbiol.*, 2016, **16**, 216.
108 L. de Sousa Eduardo, T. C. Farias, S. B. Ferreira, P. B. Ferreira, Z. N. Lima and S. B. Ferreira, Antibacterial Activity and Time-kill Kinetics of Positive Enantiomer of α-pinene Against Strains of Staphylococcus aureus and Escherichia coli, *Curr. Top. Med. Chem.*, 2018, **18**, 917–924.
109 S. Liu, R. J. Ono, H. Wu, J. Y. Teo, Z. C. Liang, K. Xu, *et al.*, Highly potent antimicrobial polyionenes with rapid killing kinetics, skin biocompatibility and in vivo bactericidal activity, *Biomaterials*, 2017, **127**, 36–48.
110 J. Li, Y. Wei, J. Wang, Y. Li, G. Shao, Z. Feng, *et al.*, Characterization of Mutations in DNA Gyrase and Topoisomerase IV in Field Strains and In Vitro Selected Quinolone-Resistant Mycoplasma hyorhinis Mutants, *Antibiotics*, 2022, **11**, 494.
111 M. D. Huband, P. A. Bradford, L. G. Otterson, G. S. Basarab, A. C. Kutschke, R. A. Giacobbe, *et al.*, *In Vitro* Antibacterial Activity of AZD0914, a New Spiropyrimidinetrione DNA Gyrase/Topoisomerase Inhibitor with Potent Activity against Gram-Positive, Fastidious Gram-Negative, and Atypical Bacteria, *Antimicrob. Agents Chemother.*, 2015, **59**, 467–474.
112 L. Coronado, X.-Q. Zhang, D. Dorta, N. Escala, L. M. Pineda, M. G. Ng, *et al.*, Semisynthesis, Antiplasmodial Activity, and Mechanism of Action Studies of Isocoumarin Derivatives, *J. Nat. Prod.*, 2021, **84**, 1434–1441.
113 S. Roychoudhury, K. M. Makin, T. L. Twinem, D. T. Stanton, S. L. Nelson and C. E. Catrenich, Development and Use of a High-Throughput Bacterial DNA Gyrase Assay to Identify Mammalian Topoisomerase II Inhibitors with Whole-Cell Anticancer Activity, *SLAS Discov.*, 2003, **8**, 157–163.
114 M. Mora-Pale, N. Bhan, S. Masuko, P. James, J. Wood, S. McCallum, *et al.*, Antimicrobial mechanism of

resveratrol-trans-dihydrodimer produced from peroxidase-catalyzed oxidation of resveratrol, *Biotechnol. Bioeng.*, 2015, **112**, 2417–2428.

115 E. A. Fayed, M. A. Ebrahim, U. Fathy, A. M. Elawady, W. S. Khalaf and T. M. Ramsis, Pyrano-coumarin hybrids as potential antimicrobial agents against MRSA strains: Design, synthesis, ADMET, molecular docking studies, as DNA gyrase inhibitors, *J. Mol. Struct.*, 2024, **1295**, 136663.

116 E. A. Fayed, E. M. E. Al-Arab, A. S. Saleh, A. H. Bayoumi and Y. A. Ammar, Design, synthesis, in silico studies, in vivo and in vitro assessment of pyridones and thiazolidinones as anti-inflammatory, antipyretic and ulcerogenic hits, *J. Mol. Struct.*, 2022, **1260**, 132839.

117 M. Ganesan, J. Sekar, S. Palani Kandasamy and P. Srinivasan, Design, synthesis, spectral characterization, in silico ADMET studies, molecular docking, antimicrobial activity, and anti breast cancer activity of 5,6-dihydrobenzo[H]quinazolines, *J. Mol. Struct.*, 2024, **1296**, 136771.

118 S. Ramkumar and R. Ramarajan, Design, Synthesis, Spectral Characterization, Antioxidant Activity, Molecular Docking and in silico ADMET Studies of 1, 3 Oxazepines, *ChemistrySelect*, 2023, **8**, e202204818.

119 S. Ramkumar and R. Ramarajan, Design, synthesis, spectral characterization, multiple-biological activities, docking and in silico ADMET studies of thiazolidinones, *Results Chem.*, 2023, **5**, 100861.

120 A. K. Das, P. Paul, M. P. Pranto, M. J. Hassan, K. Saha and M. E. Hossain, Design, synthesis, characterization, antimicrobial activity, cytotoxicity, molecular docking, and in-silico ADMET analysis of the novel cefuroxime derivatives, *Eur. J. Med. Chem. Rep.*, 2024, **10**, 100129.

121 P. F. Lamie and J. N. Philoppes, Design, synthesis, stereochemical determination, molecular docking study, in silico pre-ADMET prediction and anti-proliferative activities of indole-pyrimidine derivatives as Mcl-1 inhibitors, *Bioorg. Chem.*, 2021, **116**, 105335.

122 S. Hussein, E. A. Fayed, A. Ragab, M. S. Abusaif, Y. A. Ammar, R. El-Sayed Mansou, *et al.*, Flufenamic acid-based sulfonohydrazide and acetamide derivatives NSAI as inhibitors of multi-targets COX-1/COX-2/5-LOX: design, synthesis, in silico ADMET and binding mode studies, *BMC Chem.*, 2025, **19**, 271.

123 E. A. Fayed, M. A. A. Najm, K. H. Oudah, M. A. Ebrahim, N. A. Gohar, K. Abu-Elfotuh, *et al.*, From bench to brain: novel thieno-oxazine hybrids as potent pleiotropic anti-Alzheimer's agents with in vivo/in vitro validation and in silico insights, *J. Enzyme Inhib. Med. Chem.*, 2026, **41**, 2598741.

124 S. Hertig, T. D. Goddard, G. T. Johnson and T. E. Ferrin, Multidomain Assembler (MDA) Generates Models of Large Multidomain Proteins, *Biophys. J.*, 2015, **108**, 2097–2102.

125 J. E. Chen, C. C. Huang and T. E. Ferrin, RRDistMaps: a UCSF Chimera tool for viewing and comparing protein distance maps, *Bioinformatics*, 2015, **31**, 1484–1486.

126 C. C. Huang, E. C. Meng, J. H. Morris, E. F. Pettersen and T. E. Ferrin, Enhancing UCSF Chimera through web services, *Nucleic Acids Res.*, 2014, **42**, W478–W484.

127 Z. Yang, K. Lasker, D. Schneidman-Duhovny, B. Webb, C. C. Huang, E. F. Pettersen, *et al.*, UCSF Chimera, MODELLER, and IMP: an integrated modeling system, *J. Struct. Biol.*, 2012, **179**, 269–278.

128 M. D. Hanwell, D. E. Curtis, D. C. Lonie, T. Vandermeersch, E. Zurek and G. R. Hutchison, Avogadro: an advanced semantic chemical editor, visualization, and analysis platform, *J. Cheminf.*, 2012, **4**, 17.

129 A. M. Korkor, H. S. Abbass, A. H. Ahmed, A. M. Mansour, T. M. Ramsis, R. H. Elkousy, *et al.*, Insulinotropic and anti-obesity properties of ethno-medicinal plants: pharmacology-based and in-silico predictions, *Nat. Prod. Res.*, 2025, 1–10.

130 R. Huey and G. M. Morris, *Using AutoDock 4 with AutoDocktools: a Tutorial*, The Scripps Research Institute, USA, 2008, vol. 8, pp. 54–56.

131 Y. A. Ammar, E. A. Fayed, A. H. Bayoumi, M. A. Saleh and M. E. El-Araby, Design and synthesis of pyridine-amide based compounds appended naproxen moiety as anti-microbial and anti-inflammatory agents, *Am. J. PharmTech Res.*, 2015, **5**, 245–273.

132 H. I. Ali, K. Tomita, E. Akaho, H. Kambara, S. Miura, H. Hayakawa, *et al.*, Antitumor studies. Part 1: Design, synthesis, antitumor activity, and AutoDock study of 2-deoxo-2-phenyl-5-deazaflavins and 2-deoxo-2-phenylflavin-5-oxides as a new class of antitumor agents, *Bioorg. Med. Chem.*, 2007, **15**, 242–256.

133 A. Mai, S. Massa, R. Ragno, I. Cerbara, F. Jesacher, P. Loidl, *et al.*, 3-(4-Aroyl-1-methyl-1H-2-pyrrolyl)-N-hydroxy-2-alkylamides as a New Class of Synthetic Histone Deacetylase Inhibitors. 1. Design, Synthesis, Biological Evaluation, and Binding Mode Studies Performed through Three Different Docking Procedures, *J. Med. Chem.*, 2003, **46**, 512–524.

134 H. A. Elseedy, C. Kiriacos and T. M. Ramsis, Molecular Modeling and Drug Development, in *Applied Biotechnology and Bioinformatics*, 2024, pp. 109–137.

135 E. W. Bell and Y. Zhang, DockRMSD: an open-source tool for atom mapping and RMSD calculation of symmetric molecules through graph isomorphism, *J. Cheminf.*, 2019, **11**, 40.

136 S. Bondock, T. Albarqi, M. M. Abdou and N. M. Mohamed, Computational insights into novel benzenesulfonamide-1,3,4-thiadiazole hybrids as a possible VEGFR-2 inhibitor: design, synthesis and anticancer evaluation with molecular dynamics studies, *New J. Chem.*, 2023, **47**, 20602–20618.